

# A discontinuous Galerkin formulation of non-linear Kirchhoff-Love shells.

L. Noels<sup>†,\*</sup>

*University of Liège, Computational & Multiscale Mechanics of Materials,  
Chemin des Chevreuils 1, B-4000 Liège, Belgium*

## SUMMARY

Discontinuous Galerkin methods provide a means of weakly enforcing the continuity of the unknown-field derivatives and have particular appeal in problems involving high order derivatives. This feature has previously been successfully exploited [L. Noels and R. Radovitzky, *CMAME*, 2008] to develop a formulation of linear Kirchhoff-Love shells considering only the membrane and bending responses. In this proposed one-field method - the displacements are the only unknowns, while the displacement field is continuous, the continuity in the displacement derivative between two elements is weakly enforced by recourse to a discontinuous Galerkin formulation. It is the purpose of the present paper to extend this formulation to finite deformations and non-linear elastic behaviors. While the initial linear formulation was relying on the direct linear computation of the effective membrane stress and effective bending couple-stress from the displacement field at the mid-surface of the shell, the non-linear formulation considered implies the evaluation of the general stress tensor across the shell thickness, leading to a reformulation of the internal forces of the shell. Nevertheless, since the interface terms resulting from

---

\*Correspondence to: L.Noels@ulg.ac.be

<sup>†</sup>Postdoctoral Scholar at the Belgian National Fund for Scientific Research (FNRS)

*Received*

*Revised*

the discontinuous Galerkin method involve only the resultant couple-stress at the edges of the shells, the extension to non-linear deformations is straightforward. Copyright © 2008 John Wiley & Sons, Ltd.

KEY WORDS: Kirchhoff-Love shell; discontinuous Galerkin method; non-linear elasticity; finite deformations

## 1. INTRODUCTION

Kirchhoff-Love assumption for shells constrains the surface normal to remain perpendicular to the shell. This omission of the shearing allows the formulation of the problem as a one-field displacement method [1], but leads to weak formulations involving high order derivatives. These high-order derivative terms require polynomial approximations of the displacement field with the same degree of continuity, which, for finite-elements methods, corresponds to the use of shape-functions fulfilling the high-order continuity requirements.

Although Zienkiewicz and Taylor [2] introduced  $C^1$  continuous elements, their shapes and their numbers of degrees of freedom needed put serious limitations on their usability and scalability. Therefore, alternative one-field displacement formulations were developed in the general 3D-case. One solution developed for Kirchhoff-Love shells is the subdivision method based on splines approximation of the surface [1, 3].

Another solution is to enforce weakly the high-order continuity requirements by recourse to spatially-discontinuous Galerkin (DG) methods. This weak enforcement corresponds to allow for jumps at the inter-element boundaries, while consistency and stability of the formulation are ensured by boundary integral terms. If, in the context of solid mechanics, DG can be developed

for problems involving discontinuities in the unknown field, see [4] for linear elasticity, [5–8] for non-linear elasticity and [9] for plasticity, it has also been exploited in the case of  $\mathcal{C}^0$  displacement unknown fields, which suffer from discontinuities in their derivative. This method has recently been exploited for applications to beams and plates [10–12] and for theories of damage [13, 14]. In the resulting one-field formulations, the jump discontinuities can be related to the unknown fields and to their derivatives [11], or to the derivatives alone [10, 12].

Following this idea of using such a continuous one-field formulation, we have recently developed a discontinuous Galerkin formulation for linear Kirchhoff-Love shells [15]. In this formulation, the unknown field is continuous, and the continuity in its derivative is weakly ensured by recourse to a DG method. Toward this end, the membrane and bending responses are considered, while the shearing is neglected. A similar approach has also been proposed in [16], the main difference being the use of lifting operators in [16], while the discontinuous Galerkin method is reduced to an interior penalty method in [15].

The kinematics of the shell is described within the framework in [17, 18], but the surface normal is assumed to remain perpendicular to the shell. This omission of the shearing allows the formulation of the problem as a one-field displacement method as it has been previously shown in [1]. In this proposed formulation, while the displacement field is continuous, discontinuities in the displacement derivative between two elements are accounted for by considering the variation in their normal direction. Consistency, optimal convergence rate and stability are ensured by the addition of the integration on the element-boundaries of respectively the resultant moment, its symmetric counterpart and a (sufficiently large) quadratic term. In particular, the convergence rate of the method in the energy norm has been shown to be one order lower than the degree of the polynomial approximation used, and the convergence rate

in the  $L^2$ -norm has been demonstrated to be one order higher than this polynomial degree, which motivated the use of quadratic and cubic elements, [15].

This method was also shown to reduce locking inherent to finite-element discretizations, especially for thin structures like beams, plates or shells, for which the locking results in excessive stiffness when the membrane and bending modes are mixed. While this is generally solved by considering reduced integration [19,20], or by using a mixed formulation sometimes combined with enhanced assumed strains methods [17,18,21,22], it has been shown in [15] that when considering 4-Gauss-point bi-cubic quadrangles or 16-Gauss-point bi-cubic quadrangles, the formulation does not suffer from locking unless the stabilization parameter weighting quadratic terms tends to infinity.

Naturally, this discontinuous Galerkin method for linear Kirchhoff-Love shells is now extended to finite deformations and or finite displacements. Indeed, the formulation presented in [15] is strictly linear, and even if the one presented in [16] accounts for finite displacements and rotations, the method has not been extended yet to non-linear material behavior. The present paper is therefore focusing on this extension.

Since finite deformations imply modification of the shell thickness, the starting point of the developed method is the one of Simo *et al.* [23] who introduced the thickness ratio as a local unknown. As in the linear case, the surface normal is assumed to remain perpendicular to the shell, thus omitting shearing, which allows the formulation of the problem as a one-field displacement method. The thickness ratio is determined on all through-the-thickness Simpson points by stating a plane-stress state. The resulting stress field is therefore integrated, with a Simpson rule, on the thickness to evaluate the resultant membrane and bending responses of the shell.

Integration by parts on each shell elements of the resulting equations leads to inter-element boundary terms due to the discontinuities in the shell normal direction. After defining a numerical flux to replace this boundary terms, symmetrising the equations and stabilizing the formulation by recourse to quadratic interface terms in the jumps, a new discontinuous Galerkin formulation is obtained, which, in the linear range, reduces to the formulation proposed in [15].

The organization of the present paper is the following. In section 2 the continuum model for a thin body experiencing finite deformations and/or displacements is described. Focus is restricted to the case where shell normal remains perpendicular to the mid-surface during the deformation process. Shearing arising from the shell-thickness deformation gradient is also neglected. The resulting one-field discontinuous Galerkin weak formulation of this problem is presented in section 3. Although this formulation is consistent for finite deformations, stability and convergence rate are demonstrated under the restriction of linearization of the equations. Indeed the when linearized the set of governing equations reduces to the linear formulation previously proposed and therefore inherits its properties. In particular, the method is stable, provided that a quadratic term is considered and that the stabilization parameter is larger than a constant which depends only on the polynomial approximation, and on the element shape. Moreover, for a polynomial approximation of degree  $k$  and assuming the exact solution belongs to  $H^{k+1}$ , the convergence rate of the method in the energy norm, with respect to the mesh-size, is equal to  $k - 1$ . Under the same assumption, the convergence rate in the  $L^2$ -norm, is equal to  $k + 1$  if  $k > 2$  and is quadratic for quadratic elements. This method is implemented by recourse to interface elements integrating the inter-elements boundary terms, and numerical examples illustrate the excellent behavior of the method in section 4. The numerical tests are

conventional applications for non-linear shells proposed in numerous publications, [24–33, e.g.]. Loading applied in this papers on the structure are the most dramatic that can be found in this literature, which demonstrated the robustness of the method to capture accurately finite deformations, and rotations.

## 2. CONTINUUM MECHANICS OF KIRCHHOFF-LOVE SHELLS

In this section, the kinematics of a thin body is described, with particular attention paid to the case of the Kirchhoff-Love assumption, which neglects the shearing across the thickness. Under this assumption, the governing equation of the body can be rewritten in terms of resultant stress vectors and resultant torque vectors, which depend only on the deformation of the mid-surface of the shell. Finally, a non-linear elastic behavior is considered and is developed in the convected basis in order to ease the strict enforcement of the plane-stress assumed state.

### 2.1. Kinematics of the Kirchhoff-Love shell

[Figure 1 about here.]

A thin body can be described by considering its mid-surface section as a Cosserat plane  $\mathcal{A}_0$  and a third coordinate, representing the thickness, and belonging to the interval  $[h_{\min 0}; h_{\max 0}]$ . Subscript 0 refers to the initial thickness of the shell. In the reference frame  $\mathbf{E}_I$ , this representation is written  $\boldsymbol{\xi} = \xi^I \mathbf{E}_I$ , with  $(\xi^1, \xi^2) \in \mathcal{A}_0$ ,  $\xi^3 \in [h_{\min 0}; h_{\max 0}]$ , for  $I = 1, 2, 3$ . Hereinafter, a subscript will be used to refer to values expressed in the considered basis, while a superscript will be used to refer to values expressed in the conjugate basis. Of course, for the initial frame,  $\mathbf{E}_I = \mathbf{E}^I$ . Roman letters as a subscript or superscript substitute for integers between one and three, while Greek letters substitute for integers one or two.

The representation of the body in the inertial frame is illustrated in Fig. 1. A configuration  $\mathcal{S}$  of the shell is described by using  $\varphi(\xi^1, \xi^2)$  the mapping of the mid-surface and by the unit vector  $\mathbf{t}$ , which is the director of the mid-surface ( $\|\mathbf{t}\| = 1$ ). Therefore, the position  $\mathbf{x}$  of the points in this configuration  $\mathcal{S}$  can be defined by the mapping  $\mathbf{x} = \Phi(\xi^I) = \varphi(\xi^\alpha) + \xi^3 \lambda_h \mathbf{t}(\xi^\alpha)$ . In this last equations,  $\lambda_h = \frac{h_{\max} - h_{\min}}{h_{\max 0} - h_{\min 0}}$  corresponds to the thickness stretch of the shell resulting from the Cosserat plane deformation. Its introduction follows the argumentation of Simo *et al.* [23].

By convention,  $\mathcal{S}$  refers to the current configuration of the shell, while the reference configuration  $\mathcal{S}_0$  is obtained by the mapping  $\Phi_0$ . The transformation  $\chi = \Phi \circ \Phi_0^{-1}$  between these two configurations is characterized by the two-point deformation gradient

$$\mathbf{F} = \nabla \Phi \circ [\nabla \Phi_0]^{-1}, \quad (1)$$

with a positive Jacobian.

In this last relation, the tangent map  $\nabla \Phi$  can be evaluated as

$$\nabla \Phi = \mathbf{g}_i \otimes \mathbf{E}^i, \quad \text{with} \quad (2)$$

$$\mathbf{g}_\alpha = \frac{\partial \Phi}{\partial \xi^\alpha} = \varphi_{,\alpha} + \xi^3 \lambda_{h,\alpha} \mathbf{t} + \xi^3 \mathbf{t} \lambda_{h,\alpha} \quad \text{and} \quad \mathbf{g}_3 = \frac{\partial \Phi}{\partial \xi^3} = \lambda_h \mathbf{t}, \quad (3)$$

defining the convected basis. This convected basis satisfies the relation  $\mathbf{g}_i = \nabla \Phi \mathbf{E}_i$ , and its conjugate basis satisfies  $\mathbf{g}^i = \nabla \Phi^{-T} \mathbf{E}^i$ . Using these last results, the deformation gradient (1) can be rewritten

$$\mathbf{F} = \varphi_{,\alpha} \otimes \mathbf{g}_0^\alpha + \xi^3 \lambda_{h,\alpha} \mathbf{t} \otimes \mathbf{g}_0^\alpha + \lambda_h \mathbf{t} \otimes \mathbf{g}_0^3, \quad (4)$$

where the gradient of the variation of thickness, accounted for by the term  $\xi^3 \lambda_{h,\alpha} \mathbf{t} \otimes \mathbf{g}_0^\alpha$  has been neglected. This gradient of thickness deformation would correspond to a shearing, and

can therefore be omitted, since this omission introduces an error of the same order as the Kirchhoff-Love assumption. The Jacobian of this deformation mapping is denoted by

$$J = \det(\mathbf{F}) = \frac{j}{j_0}, \text{ with } j = \det(\nabla\Phi) = \mathbf{g}_3 \cdot (\mathbf{g}_1 \wedge \mathbf{g}_2), \quad (5)$$

while the Jacobian related to the deformation of the mid-surface is computed by

$$\bar{J} = \frac{\bar{j}}{j_0}, \text{ with } \bar{j} = \|\varphi_{,1} \wedge \varphi_{,2}\|. \quad (6)$$

Since the particular case of Kirchhoff-Love shells corresponds to neglect shearing deformations, the unit vector  $\mathbf{t}$  remains always perpendicular to  $\varphi_{,\alpha}$  with

$$\mathbf{t} = \frac{\varphi_{,1} \wedge \varphi_{,2}}{\|\varphi_{,1} \wedge \varphi_{,2}\|}. \quad (7)$$

Finally, if  $e_{ijk}$  is the permutation tensor, the gradient of the unit vector (7) can be decomposed into

$$\mathbf{t}_{,\alpha} = \frac{e_{\beta\gamma 3}}{j} \varphi_{\beta\alpha} \wedge \varphi_{,\gamma} - \frac{\mathbf{t}}{j} e_{\beta\gamma 3} (\varphi_{,\beta\alpha} \wedge \varphi_{,\gamma}) \cdot \mathbf{t}. \quad (8)$$

## 2.2. Governing equations of the shell

Following [17,18], the integration on the thickness of the Cauchy stress tensor  $\boldsymbol{\sigma}$  leads to the definition of

$$\mathbf{n}^\alpha = \frac{1}{j} \int_{h_{\min 0}}^{h_{\max 0}} \boldsymbol{\sigma} \mathbf{g}^\alpha \det(\nabla\Phi) d\xi^3 = \frac{1}{j} \int_{h_{\min 0}}^{h_{\max 0}} \boldsymbol{\tau} \mathbf{g}^\alpha \det(\nabla\Phi_0) d\xi^3, \quad (9)$$

$$\begin{aligned} \mathbf{m}^\alpha &= \frac{\lambda_h}{j} \mathbf{t} \wedge \int_{h_{\min 0}}^{h_{\max 0}} \xi^3 \boldsymbol{\sigma} \mathbf{g}^\alpha \det(\nabla\Phi) d\xi^3 = \frac{\lambda_h}{j} \mathbf{t} \wedge \int_{h_{\min 0}}^{h_{\max 0}} \xi^3 \boldsymbol{\tau} \mathbf{g}^\alpha \det(\nabla\Phi_0) d\xi^3 \\ &= \lambda_h \mathbf{t} \wedge \tilde{\mathbf{m}}^\alpha, \text{ and} \end{aligned} \quad (10)$$

$$\mathbf{l} = \frac{1}{j} \int_{h_{\min 0}}^{h_{\max 0}} \boldsymbol{\sigma} \mathbf{g}^3 \det(\nabla\Phi) d\xi^3 = \frac{1}{j} \int_{h_{\min 0}}^{h_{\max 0}} \boldsymbol{\tau} \mathbf{g}^3 \det(\nabla\Phi_0) d\xi^3, \quad (11)$$

respectively the resultant stress vector, the resultant torque vector and the resultant across-the-thickness stress vector. For convenience when developing the material law behavior, see

section 2.3, these last three equations have been rewritten in terms of the Kirchhoff stress tensor  $\boldsymbol{\tau} = J\boldsymbol{\sigma}$ .

Therefore, the governing equations of a thin body are also obtained by integrating on the thickness the equations of force and moment equilibrium, leading to

$$\frac{1}{j} (\bar{j}\mathbf{n}^\alpha)_{,\alpha} + \mathbf{n}^{\mathcal{A}_0} = 0 \quad \text{on } \mathcal{A}_0 \text{ and} \quad (12)$$

$$\frac{1}{j} (\bar{j}\tilde{\mathbf{m}}^\alpha)_{,\alpha} - \mathbf{l} + \lambda \mathbf{t} + \tilde{\mathbf{m}}^{\mathcal{A}_0} = 0 \quad \text{on } \mathcal{A}_0, \quad (13)$$

where  $\lambda$  is an undefined pressure, where  $\mathbf{n}^{\mathcal{A}_0}$  is the resultant external surface traction and where  $\tilde{\mathbf{m}}^{\mathcal{A}_0}$  is the resultant external torque by unit surface. The equations correspond to respectively (94) and (105), which are established in appendix I. Terms  $\mathbf{n}^{\mathcal{A}_0}$  and  $\tilde{\mathbf{m}}^{\mathcal{A}_0}$  depend both on the body force  $\mathbf{B}$  and on the true physical surface tractions applied to the thin body surfaces:

$$\mathbf{n}^{\mathcal{A}_0} = \frac{1}{j} \left[ (\boldsymbol{\sigma} \mathbf{g}^3 \det(\nabla \Phi))_{h_{\min 0}}^{h_{\max 0}} + \int_{h_{\min 0}}^{h_{\max 0}} \frac{\rho_0}{\rho} \mathbf{B} \det(\nabla \Phi) d\xi^3 \right], \text{ and} \quad (14)$$

$$\tilde{\mathbf{m}}^{\mathcal{A}_0} = \frac{1}{j} \left[ (\xi^3 \boldsymbol{\sigma} \mathbf{g}^3 \det(\nabla \Phi))_{h_{\min 0}}^{h_{\max 0}} + \int_{h_{\min 0}}^{h_{\max 0}} \xi^3 \frac{\rho_0}{\rho} \mathbf{B} \det(\nabla \Phi) d\xi^3 \right]. \quad (15)$$

This set of governing equations is accompanied by boundary conditions applied on the boundary  $\partial \mathcal{A}_0$  of the mid-surface  $\mathcal{A}_0$ . This boundary  $\partial \mathcal{A}_0$  is decomposed into a part  $\partial_T \mathcal{A}_0$  where the unit vector is constraint  $\bar{\mathbf{t}}$  and into a part  $\partial_M \mathcal{A}_0$  where the applied torque is  $\bar{\tilde{\mathbf{m}}}$ , such that

$$\mathbf{t} = \bar{\mathbf{t}} \quad \forall (\xi^1, \xi^2) \in \partial_T \mathcal{A}_0, \quad (16)$$

$$\tilde{\mathbf{m}}^\alpha \nu_\alpha = \bar{\tilde{\mathbf{m}}} \quad \forall (\xi^1, \xi^2) \in \partial_M \mathcal{A}_0, \quad (17)$$

where  $\boldsymbol{\nu} = \nu_\alpha \boldsymbol{\varphi}^\alpha$  is the external normal of the mid-surface boundary (in this last expression  $\boldsymbol{\varphi}^\alpha$  denotes, with an abuse of notation, the conjugate basis to  $\boldsymbol{\varphi}_{,\alpha}$ ). This boundary  $\partial \mathcal{A}_0$  is

also decomposed into a part  $\partial_U \mathcal{A}_0$  where the position  $\bar{\varphi}$  is known and into a part  $\partial_N \mathcal{A}_0$  where the traction is constrained to  $\bar{\mathbf{n}}$ , with

$$\varphi = \bar{\varphi} \quad \forall (\xi^1, \xi^2) \in \partial_U \mathcal{A}_0, \quad (18)$$

$$\mathbf{n}^\alpha \nu_\alpha = \bar{\mathbf{n}} \quad \forall (\xi^1, \xi^2) \in \partial_N \mathcal{A}_0. \quad (19)$$

The decomposition of the boundary satisfies

$$\partial_T \mathcal{A}_0 \cap \partial_M \mathcal{A}_0 = 0 \quad \text{and} \quad \partial_T \mathcal{A}_0 \cup \partial_M \mathcal{A}_0 = \partial \mathcal{A}_0, \quad (20)$$

$$\partial_U \mathcal{A}_0 \cap \partial_N \mathcal{A}_0 = 0 \quad \text{and} \quad \partial_U \mathcal{A}_0 \cup \partial_N \mathcal{A}_0 = \partial \mathcal{A}_0. \quad (21)$$

### 2.3. Constitutive behavior

The set of governing Eqs. (12-13, 16-19) is completed by a constitutive law relating the deformation to the stresses. In this paper a non-linear elastic response is assumed. Toward this end, an energy potential per unit undeformed volume  $W(\mathbf{C})$  is defined and depends only on the right Cauchy tensor  $\mathbf{C} = \mathbf{F}^T \mathbf{F}$ . Owing to the existence of this internal potential, the Kirchhoff stress tensor  $\boldsymbol{\tau}$  can be computed on the shell thickness by

$$\boldsymbol{\tau} = \frac{\partial W}{\partial \mathbf{F}} \mathbf{F}^T = \mathbf{P} \mathbf{F}^T, \quad (22)$$

where  $\mathbf{P} = \frac{\partial W}{\partial \mathbf{F}}$  is the first Piola-Kirchhoff stress tensor.

Since the shell assumption corresponds to a plane-stress state in the convected basis  $\mathbf{g}_i$ , it is convenient to develop the constitutive model in this basis, see [3]. Toward this end, the right Cauchy tensor and the Kirchhoff stress tensor are rewritten

$$\mathbf{C} = \mathbf{g}_i \cdot \mathbf{g}_j \mathbf{g}_0^i \otimes \mathbf{g}_0^j = \mathbf{g}_{ij} \mathbf{g}_0^i \otimes \mathbf{g}_0^j, \quad (23)$$

$$\boldsymbol{\tau} = \tau^{ij} \mathbf{g}_i \otimes \mathbf{g}_j = 2 \frac{\partial W}{\partial \mathbf{g}_{ij}} \mathbf{g}_i \otimes \mathbf{g}_j. \quad (24)$$

The main advantage of using the Kirchhoff stress tensor becomes obvious since the plane-stress assumption is obtained by enforcing

$$\tau^{33} = 2 \frac{\partial W}{\partial g_{33}} = 0, \quad (25)$$

all across the shell thickness.

Since  $\lambda_{h,\alpha}$  is neglected and since the Kirchhoff-Love assumption leads to  $\mathbf{t},\alpha \cdot \mathbf{t} = 0$ , the deformation gradient (4) has no component along  $\alpha 3$  and  $3\alpha$  in the convected basis. Therefore, for elasticity, or J2-plasticity, the Kirchhoff stress reads

$$\tau^{i3} = \tau^{3i} = 0, \quad (26)$$

and resultant vectors (9-11) can be rewritten

$$\mathbf{n}^\alpha = \frac{1}{j} \int_{h_{\min 0}}^{h_{\max 0}} \tau^{\beta\alpha} \mathbf{g}_\beta \det(\nabla \Phi_0) d\xi^3, \quad (27)$$

$$\tilde{\mathbf{m}}^\alpha = \frac{1}{j} \int_{h_{\min 0}}^{h_{\max 0}} \xi^3 \tau^{\beta\alpha} \mathbf{g}_\beta \det(\nabla \Phi_0) d\xi^3, \text{ and} \quad (28)$$

$$\mathbf{l} = \frac{1}{j} \int_{h_{\min 0}}^{h_{\max 0}} \tau^{i3} \mathbf{g}_i \det(\nabla \Phi_0) d\xi^3 = 0. \quad (29)$$

The evaluations of the resultant stress vectors (9) and resultant torque vectors (10) are performed with a 11-point Simpson integration. At each Simpson point  $p$ , Newton-Raphson iterations are performed on the local thickness stretch  $\lambda_h^p$  to obtain the correct deformation gradient (4), which satisfies the plane stress requirement (25). The Kirchhoff stress tensor (24) is thus computed at each Simpson point, leading to the resultant stress vectors (9) and resultant torque vectors (10). Finally the global thickness stretch  $\lambda_h$  is obtained by the Simpson integration on the 11 local values  $\lambda_h^p$ .

### 3. DISCONTINUOUS GALERKIN FORMULATION

In this section, a framework for numerical approximation of the shell equations described above based on a  $\mathcal{C}^0$  polynomial approximation of the unknown field  $\varphi$  is proposed. In this formulation, the resulting discontinuity in the surface director  $\mathbf{t}$  is accounted for using a new discontinuous Galerkin formulation.

#### 3.1. Weak formulation of the problem

At this point, the mid-surface  $\mathcal{A}_0$  is approximated by a discretization  $\mathcal{A}_h$  into finite-elements  $\mathcal{A}_e$ , with  $\mathcal{A}_0 \simeq \mathcal{A}_h = \bigcup_e \bar{\mathcal{A}}_e$ . In this last equation,  $\bar{\mathcal{A}}_e$  is the union of the open domain  $\mathcal{A}_e$  with its boundary  $\partial\mathcal{A}_e$ . The boundary  $\partial\mathcal{A}_e$  of an element  $\mathcal{A}_e$  can be common with the boundary of  $\mathcal{A}_h$ , with

$$\begin{aligned} \partial_U\mathcal{A}_e &= \partial\mathcal{A}_e \cap \partial_U\mathcal{A}_h, & \partial_T\mathcal{A}_e &= \partial\mathcal{A}_e \cap \partial_T\mathcal{A}_h, \\ \partial_M\mathcal{A}_e &= \partial\mathcal{A}_e \cap \partial_M\mathcal{A}_h, & \text{and } \partial_N\mathcal{A}_e &= \partial\mathcal{A}_e \cap \partial_N\mathcal{A}_h. \end{aligned} \quad (30)$$

The remaining part of the boundary  $\partial\mathcal{A}_e$  is shared with another finite element and is part of the interior boundary  $\partial_I\mathcal{A}_h$ , with

$$\partial_I\mathcal{A}_e = \partial\mathcal{A}_e \setminus \partial\mathcal{A}_h = \partial\mathcal{A}_e \cap \partial_I\mathcal{A}_h, \text{ with } \partial_I\mathcal{A}_h = \bigcup_e \partial\mathcal{A}_e \setminus \partial\mathcal{A}_h. \quad (31)$$

Instead of seeking the exact solution  $\varphi$ , a polynomial approximation  $\varphi_h \in U_h^k$  constitutes the solution to the finite element problem. In this work, a continuous polynomial approximation is considered, but the derivatives of the displacement field are allowed to be discontinuous on the element boundaries, leading to the definition of the displacement manifold and of its

constrained counterpart

$$U_h^k = \{ \varphi_h \in \mathbf{H}^1(\mathcal{A}_h) \mid \varphi_h|_{\mathcal{A}_e} \in \mathbb{P}^k \quad \forall \mathcal{A}_e \in \mathcal{A}_h \} \subset U^f(\mathcal{A}_h), \quad (32)$$

$$U_{hc}^k = \left\{ \delta\varphi \in U_h^k \mid \delta\varphi|_{\partial U, \mathcal{A}_0} = 0 \right\} \subset U_c^f(\mathcal{A}_h), \quad (33)$$

with  $U^f(\mathcal{A}_h) = \mathcal{C}^0(\mathcal{A}_h) \cap \prod_e \mathbf{H}^2(\mathcal{A}_e)$  for polynomial approximations  $k > 1$  and with  $U_c^f(\mathcal{A}_h) = \left\{ \delta\varphi \in U^f(\mathcal{A}_h) \mid \delta\varphi|_{\partial U, \mathcal{A}_0} = 0 \right\}$ .

The purpose of this section is to establish a weak form of the problem stated by the set of Eqs. (12-13, 16-19) for an approximation  $\varphi_h \in U_h^k$ . Owing to the definition of this manifold, see Eq. (32), the displacement field and the test functions are continuous across element-interfaces but allow for jump discontinuities in their derivative, which has to be accounted for when establishing the new weak form of the problem.

Multiplying Eq. (12) by a test function  $\delta\varphi \in U_{hc}^k$  and Eq. (13) by the corresponding variation of unit vector  $\lambda_h \delta\mathbf{t} = \lambda_h \mathbf{t}(\delta\varphi)$ , state the problem as finding  $\varphi_h \in U_h^k$  such that

$$\begin{aligned} 0 &= \sum_e \int_{\bar{\mathcal{A}}_e} (\bar{j}\mathbf{n}^\alpha(\varphi_h))_{,\alpha} \cdot \delta\varphi d\mathcal{A}_0 + \int_{\mathcal{A}_h} \mathbf{n}^{\mathcal{A}_0} \cdot \delta\varphi \bar{j} d\mathcal{A}_0 + \\ &\quad \sum_e \int_{\bar{\mathcal{A}}_e} \left[ (\bar{j}\tilde{\mathbf{m}}^\alpha(\varphi_h))_{,\alpha} - \bar{j}\mathbf{l} \right] \cdot \delta\mathbf{t} \lambda_h d\mathcal{A}_0 + \int_{\mathcal{A}_h} \tilde{\mathbf{m}}^{\mathcal{A}_0} \cdot \delta\mathbf{t} \lambda_h \bar{j} d\mathcal{A}_0 \quad \forall \delta\varphi \in U_{hc}^k. \end{aligned} \quad (34)$$

Integration by parts of these integrals followed by the application of the Gauss theorem leads to

$$\begin{aligned} 0 &= - \sum_e \int_{\bar{\mathcal{A}}_e} \bar{j}\mathbf{n}^\alpha(\varphi_h) \cdot \delta\varphi_{,\alpha} d\mathcal{A}_0 + \sum_e \int_{\partial\mathcal{A}_e} \bar{j}\mathbf{n}^\alpha(\varphi_h) \cdot \delta\varphi \nu_\alpha d\mathcal{A}_0 + \int_{\mathcal{A}_h} \mathbf{n}^{\mathcal{A}_0} \cdot \delta\varphi \bar{j} d\mathcal{A}_0 - \\ &\quad \sum_e \int_{\bar{\mathcal{A}}_e} \bar{j}\tilde{\mathbf{m}}^\alpha(\varphi_h) \cdot (\delta\mathbf{t}\lambda_h)_{,\alpha} d\mathcal{A}_0 + \sum_e \int_{\partial\mathcal{A}_e} \bar{j}\tilde{\mathbf{m}}^\alpha(\varphi_h) \cdot \delta\mathbf{t}\lambda_h \nu_\alpha d\mathcal{A}_0 - \\ &\quad \sum_e \int_{\bar{\mathcal{A}}_e} \bar{j}\mathbf{l} \cdot \delta\mathbf{t}\lambda_h d\mathcal{A}_0 + \int_{\mathcal{A}_h} \tilde{\mathbf{m}}^{\mathcal{A}_0} \cdot \delta\mathbf{t}\lambda_h \bar{j} d\mathcal{A}_0 \quad \forall \delta\varphi \in U_{hc}^k. \end{aligned} \quad (35)$$

In this previous equation, test functions have been chosen as  $\lambda_h \delta\mathbf{t}$ , while the variations of  $\mathbf{t}\delta\lambda_h$  have been omitted. Indeed, although this variation could lead to a missing equation,

in this paper, this equation is substituted by the enforcement of the plane-stress assumption while solving the constitutive model, see section 2.3. Variation  $\delta\lambda_h$  will therefore be omitted in the remaining parts of this work.

When analyzing the boundary integrals in Eq. (35), it appears that the contribution involving the scalar product with  $\delta\varphi$  has the same meaning as for continuous Galerkin methods. Indeed, since  $\delta\varphi \in \mathcal{C}^0(\mathcal{A}_h)$ , and since for the exact solution  $\mathbf{n}^\alpha$  is also continuous, the following substitution satisfies the consistency requirement:

$$\sum_e \int_{\partial\mathcal{A}_e} \bar{j}\mathbf{n}^\alpha(\varphi_h) \cdot \delta\varphi\nu_\alpha d\mathcal{A}_0 \rightarrow \int_{\partial\mathcal{A}_h} \bar{j}\mathbf{n}^\alpha(\varphi_h) \cdot \delta\varphi\nu_\alpha d\mathcal{A}_0. \quad (36)$$

By contrast, the contribution involving the tensorial product with  $\delta\mathbf{t}$  requires particular attention since it is discontinuous across interelement boundaries. Since only the  $\mathcal{C}^0$  continuity is ensured across  $\partial_I\mathcal{A}_h$ , jump  $[[\bullet]]$  and mean  $\langle\bullet\rangle$  operators are defined on the space of the trace  $\mathbf{TR}(\partial_I\mathcal{A}_h) = \prod_e \mathbf{L}^2(\partial_I\mathcal{A}_e)$  of vectors that can take multiple values on this boundary, with

$$[[\bullet]] = \bullet^+ - \bullet^-, \text{ and} \quad (37)$$

$$\langle\bullet\rangle = \frac{1}{2}(\bullet^+ + \bullet^-). \quad (38)$$

In these relations the bullets represent generic vector fields with

$$\bullet^+ = \lim_{\varepsilon \rightarrow 0^+} \bullet(\xi^1 + \varepsilon\zeta^1, \xi^2 + \varepsilon\zeta^2) \text{ and} \quad (39)$$

$$\bullet^- = \lim_{\varepsilon \rightarrow 0^+} \bullet(\xi^1 - \varepsilon\zeta^1, \xi^2 - \varepsilon\zeta^2), \quad (40)$$

where  $\zeta^\alpha$  are the components of the outer unit normal  $\boldsymbol{\zeta}$  of  $\mathcal{A}_e$  in the basis  $\mathbf{E}_\alpha$ . These operators lead to vectors that are now belonging to  $\mathbf{L}^2(\partial_I\mathcal{A}_h)$ . It is worth noticing that if definition (37) of the jump operator is not independent of the choice of the + and - sides of an element edge, when this jump is used in combination with the outward unit normal of the - element  $\boldsymbol{\nu}^-$ , the formulation becomes consistent and independent on this choice. Although jump and mean

operators are meaningful on the interior boundary  $\partial_I \mathcal{A}_0$ , jump definition can be extended to  $\partial_T \mathcal{A}_0$  with

$$\llbracket \mathbf{t} \rrbracket = \bar{\mathbf{t}} - \mathbf{t}, \llbracket \delta \mathbf{t} \rrbracket = -\delta \mathbf{t} \text{ and } \langle \tilde{\mathbf{m}}^\alpha \rangle = \tilde{\mathbf{m}}^\alpha \text{ on } \partial_T \mathcal{A}_0. \quad (41)$$

From these definitions, the boundary term dependent on  $\delta \mathbf{t}$  is rewritten

$$\begin{aligned} \sum_e \int_{\partial \mathcal{A}_e} \bar{j} \tilde{\mathbf{m}}^\alpha(\varphi_h) \cdot \delta \mathbf{t} \lambda_h \nu_\alpha d\mathcal{A}_0 = \\ \int_{\partial \mathcal{A}_h} \bar{j} \tilde{\mathbf{m}}^\alpha(\varphi_h) \cdot \delta \mathbf{t} \lambda_h \nu_\alpha d\mathcal{A}_0 - \int_{\partial_I \mathcal{A}_h} \llbracket \bar{j} \tilde{\mathbf{m}}^\alpha(\varphi_h) \cdot \delta \mathbf{t} \lambda_h \rrbracket \nu_\alpha^- d\mathcal{A}_0. \end{aligned} \quad (42)$$

The main idea of the discontinuous Galerkin method is to address the contribution of the inter-element discontinuity terms by introducing a numerical flux  $\mathbf{h} \left( (\bar{j} \lambda_h \tilde{\mathbf{m}}^\alpha)^+, (\bar{j} \lambda_h \tilde{\mathbf{m}}^\alpha)^-, \nu_\alpha^- \right)$ , leading to the substitution

$$\int_{\partial_I \mathcal{A}_h} \llbracket \bar{j} \tilde{\mathbf{m}}^\alpha(\varphi_h) \cdot \delta \mathbf{t} \lambda_h \rrbracket \nu_\alpha^- d\mathcal{A}_0 \rightarrow \int_{\partial_I \mathcal{A}_h} \llbracket \delta \mathbf{t} \rrbracket \cdot \mathbf{h} \left( (\bar{j} \lambda_h \tilde{\mathbf{m}}^\alpha)^+, (\bar{j} \lambda_h \tilde{\mathbf{m}}^\alpha)^-, \nu_\alpha^- \right) d\mathcal{A}_0. \quad (43)$$

In principle, there is a significant freedom in the choice of this flux, but only a few expressions lead to stable and consistent formulation. These expressions have to verify

$$\mathbf{h}(\lambda_h \bar{j} \tilde{\mathbf{m}}^\alpha, \bar{j} \lambda_h \tilde{\mathbf{m}}^\alpha, \nu_\alpha) = \lambda_h \bar{j} \tilde{\mathbf{m}}^\alpha \nu_\alpha^- \text{ and} \quad (44)$$

$$\mathbf{h} \left( (\bar{j} \lambda_h \tilde{\mathbf{m}}^\alpha)^+, (\bar{j} \lambda_h \tilde{\mathbf{m}}^\alpha)^-, \nu_\alpha^- \right) = -\mathbf{h} \left( (\bar{j} \lambda_h \tilde{\mathbf{m}}^\alpha)^-, (\bar{j} \lambda_h \tilde{\mathbf{m}}^\alpha)^+, \nu_\alpha^+ \right), \quad (45)$$

where  $\bar{j} \lambda_h \tilde{\mathbf{m}}^\alpha$  is the exact continuous solution. In this paper, the following expression is adopted

$$\mathbf{h} \left( (\bar{j} \lambda_h \tilde{\mathbf{m}}^\alpha)^+, (\bar{j} \lambda_h \tilde{\mathbf{m}}^\alpha)^-, \nu_\alpha^- \right) = \nu_\alpha^- \langle \bar{j} \lambda_h \tilde{\mathbf{m}}^\alpha \rangle. \quad (46)$$

Combining Eqs. (36) to (46) allows rewriting the weak form (35) as finding  $\varphi_h \in U_h^k$  such

that

$$\begin{aligned}
& \int_{\mathcal{A}_h} \bar{j} \bar{\mathbf{n}}^\alpha (\boldsymbol{\varphi}_h) \cdot \delta \boldsymbol{\varphi}_{,\alpha} d\mathcal{A}_0 + \int_{\mathcal{A}_h} \bar{j} \bar{\mathbf{m}}^\alpha (\boldsymbol{\varphi}_h) \cdot (\delta \mathbf{t} \lambda_h)_{,\alpha} d\mathcal{A}_0 + \int_{\mathcal{A}_h} \bar{j} \bar{\mathbf{l}} \cdot \delta \mathbf{t} \lambda_h d\mathcal{A}_0 + \\
& \int_{\partial_I \mathcal{A}_h \cup \partial_T \mathcal{A}_h} \llbracket \delta \mathbf{t} \rrbracket \cdot \langle \bar{j} \lambda_h \bar{\mathbf{m}}^\alpha \rangle \nu_\alpha^- d\partial \mathcal{A}_0 = \int_{\partial_N \mathcal{A}_h} \bar{j} \bar{\mathbf{n}} \cdot \delta \boldsymbol{\varphi} d\mathcal{A}_0 + \int_{\partial_M \mathcal{A}_h} \bar{j} \bar{\mathbf{m}} \cdot \delta \mathbf{t} \lambda_h d\mathcal{A}_0 + \\
& \int_{\mathcal{A}_h} \mathbf{n}^{\mathcal{A}_0} \cdot \delta \boldsymbol{\varphi} \bar{j} d\mathcal{A}_0 + \int_{\mathcal{A}_h} \tilde{\mathbf{m}}^{\mathcal{A}_0} \cdot \delta \mathbf{t} \lambda_h \bar{j} d\mathcal{A}_0 \quad \forall \delta \boldsymbol{\varphi} \in \mathbf{U}_{hc}^k, \tag{47}
\end{aligned}$$

where the boundary conditions (17) and (19), and the definition (33) have been used.

The weak enforcement of the continuity of  $\mathbf{t}(\boldsymbol{\varphi}_h)$  on  $\partial_I \mathcal{A}_h \cup \partial_T \mathcal{A}_h$  is obtained by similar argumentation, which results into

$$\int_{\partial_I \mathcal{A}_h \cup \partial_T \mathcal{A}_h} \llbracket \mathbf{t}(\boldsymbol{\varphi}_h) \rrbracket \cdot \mathbf{h} \left( \delta (\bar{j} \lambda_h \bar{\mathbf{m}}^\alpha)^+, \delta (\bar{j} \lambda_h \bar{\mathbf{m}}^\alpha)^-, \nu_\alpha^- \right) d\partial \mathcal{A}_0 = 0. \tag{48}$$

In this last expression,  $\delta (\bar{j} \lambda_h \bar{\mathbf{m}}^\alpha)$  has to be defined. As it has been demonstrated in previous works for non-linear solid mechanics [6, 7, 9], this expression would actually depend on tangent moduli of the constitutive models since expression (10) leads to

$$\begin{aligned}
\delta (\bar{j} \bar{\mathbf{m}}^\alpha) &= \int_{h_{\min 0}}^{h_{\max 0}} \xi^3 \delta (\mathbf{P} \mathbf{F}^T \mathbf{g}^\alpha) \det (\boldsymbol{\nabla} \Phi_0) d\xi^3 = \int_{h_{\min 0}}^{h_{\max 0}} \xi^3 \frac{\partial \mathbf{P}}{\partial \mathbf{F}} \mathbf{g}_0^\alpha \otimes \delta \mathbf{F} \det (\boldsymbol{\nabla} \Phi_0) d\xi^3 \\
&= \int_{h_{\min 0}}^{h_{\max 0}} \xi^3 \frac{\partial \mathbf{P}}{\partial \mathbf{F}} \mathbf{g}_0^\alpha \otimes (\delta \boldsymbol{\varphi}_{,\alpha} \otimes \mathbf{g}_0^\alpha + \xi^3 \lambda_h \delta \mathbf{t}_{,\alpha} \otimes \mathbf{g}_0^\alpha + \lambda_h \delta \mathbf{t} \otimes \mathbf{g}_0^3) \det (\boldsymbol{\nabla} \Phi_0) d\xi^3. \tag{49}
\end{aligned}$$

But, since the purpose of this term is to ensure that Eq. (48) is energetically consistent with (47), another form of the flux can be chosen, as long as the consistency condition remains satisfied. Ideally this term should, when linearized, lead to a symmetric formulation and to the same expression as the one proposed for linear elasticity [15]. An obvious choice is to consider

the elastic behavior proposed in [23] for elasticity with finite deformations, yielding

$$\begin{aligned}
\delta(\bar{j}\lambda_h\tilde{\mathbf{m}}^\alpha) &= \delta(\bar{j}\lambda_h\tilde{m}^{\alpha\beta}\boldsymbol{\varphi}_{,\beta} + \bar{j}\lambda_h^2\tilde{m}^{3\alpha}\mathbf{t}) \\
&= \bar{j}_0\mathcal{H}_m^{\alpha\beta\gamma\delta}(\delta\boldsymbol{\varphi}_{,\gamma}\cdot\mathbf{t}_{,\delta} + \boldsymbol{\varphi}_{,\gamma}\cdot\delta\mathbf{t}_{,\delta})\boldsymbol{\varphi}_{,\beta} + \bar{j}\lambda_h\tilde{\mathbf{m}}^\alpha\cdot\boldsymbol{\varphi}_{,\beta}\delta\boldsymbol{\varphi}_{,\beta} + \\
&\quad \bar{j}_0\frac{7*E*(h_{\max}-h_{\min})^3}{240(1+\nu)}\boldsymbol{\varphi}_0^{\prime\alpha}\cdot\boldsymbol{\varphi}_0^{\prime\beta}\left(\frac{\delta\lambda_h}{\lambda_h}\right)_{,\beta}\mathbf{t} + \bar{j}\lambda_h^2\tilde{m}^{3\alpha}\delta\mathbf{t}, \quad (50)
\end{aligned}$$

where  $\tilde{m}^{\alpha\beta}$  and  $\tilde{m}^{3\alpha}$  are respectively the components of  $\tilde{\mathbf{m}}^\alpha$  along  $\boldsymbol{\varphi}_{,\beta}$  and  $\mathbf{t}/\lambda_h$ , where  $\bar{j}\lambda_h\tilde{\mathbf{m}}^\alpha\cdot\boldsymbol{\varphi}_{,\beta}\delta\boldsymbol{\varphi}_{,\beta}$ , and  $\bar{j}\lambda_h\tilde{m}^{3\alpha}\delta\mathbf{t}$  are the geometric parts of the linearization, and where

$$\begin{aligned}
\mathcal{H}_m^{\alpha\beta\gamma\delta} &= \frac{E(h_{\max}-h_{\min})^3}{12(1-\nu^2)}\left[\nu\boldsymbol{\varphi}_0^{\prime\alpha}\cdot\boldsymbol{\varphi}_0^{\prime\beta}\boldsymbol{\varphi}_0^{\prime\gamma}\cdot\boldsymbol{\varphi}_0^{\prime\delta} + \frac{1}{2}(1-\nu)\boldsymbol{\varphi}_0^{\prime\alpha}\cdot\boldsymbol{\varphi}_0^{\prime\gamma}\boldsymbol{\varphi}_0^{\prime\delta}\cdot\boldsymbol{\varphi}_0^{\prime\beta} + \right. \\
&\quad \left. \frac{1}{2}(1-\nu)\boldsymbol{\varphi}_0^{\prime\alpha}\cdot\boldsymbol{\varphi}_0^{\prime\delta}\boldsymbol{\varphi}_0^{\prime\gamma}\cdot\boldsymbol{\varphi}_0^{\prime\beta}\right] \quad (51)
\end{aligned}$$

is the linearized bending stiffness. It bears emphasizes that for a complex material behavior, in this last expression, the Young modulus  $E$  as well as the Poisson's ratio  $\nu$  are the equivalent values obtained at the current state of deformation. As it as been pointed out in [9], the stiffness matrix at the current state of deformation cannot be used, as for perfectly plastic behavior it would lead to vanishing terms. Therefore linearization (50) is not only a efficient simplification as it reduces the computational cost, but it also prevent from instabilities for such material behaviors.

Moreover, since  $\lambda_{h,\beta}$  has been neglected in the constitutive law, see equation (4), the last two terms of (50) related to  $\tilde{m}^{3\alpha}$  are omitted. Therefore, using the flux definition (46), the sum of the weak forms (47) and (48) leads to the new statement of the problem, which is finding

$\varphi_h \in U_h^k$  such that

$$\begin{aligned}
& \int_{\mathcal{A}_h} \bar{j} \bar{\mathbf{n}}^\alpha(\varphi_h) \cdot \delta \varphi_{,\alpha} d\mathcal{A}_0 + \int_{\mathcal{A}_h} \bar{j} \bar{\mathbf{m}}^\alpha(\varphi_h) \cdot (\delta \mathbf{t} \lambda_h)_{,\alpha} d\mathcal{A}_0 + \int_{\mathcal{A}_h} \bar{j} \bar{\mathbf{l}} \cdot \delta \mathbf{t} \lambda_h d\mathcal{A}_0 + \\
& \int_{\partial_I \mathcal{A}_h \cup \partial_T \mathcal{A}_h} \llbracket \delta \mathbf{t} \rrbracket \cdot \langle \bar{j} \lambda_h \bar{\mathbf{m}}^\alpha \rangle \nu_\alpha^- d\partial \mathcal{A}_0 + \int_{\partial_I \mathcal{A}_h \cup \partial_T \mathcal{A}_h} \llbracket \mathbf{t}(\varphi_h) \rrbracket \cdot \\
& \quad \langle \bar{j}_0 \mathcal{H}_m^{\alpha\beta\gamma\delta} (\delta \varphi_{,\gamma} \cdot \mathbf{t}_{,\delta} + \varphi_{,\gamma} \cdot \delta \mathbf{t}_{,\delta}) \varphi_{,\beta} + \bar{j} \lambda_h \bar{\mathbf{m}}^\alpha \cdot \varphi_{,\beta} \delta \varphi_{,\beta} \rangle \nu_\alpha^- d\partial \mathcal{A}_0 \\
& = \int_{\partial_N \mathcal{A}_h} \bar{j} \bar{\mathbf{n}} \cdot \delta \varphi d\mathcal{A}_0 + \int_{\partial_M \mathcal{A}_h} \bar{j} \bar{\mathbf{m}} \cdot \delta \mathbf{t} \lambda_h d\mathcal{A}_0 + \\
& \quad \int_{\mathcal{A}_h} \mathbf{n}^{A_0} \cdot \delta \varphi \bar{j} d\mathcal{A}_0 + \int_{\mathcal{A}_h} \bar{\mathbf{m}}^{A_0} \cdot \delta \mathbf{t} \lambda_h \bar{j} d\mathcal{A}_0 \quad \forall \delta \varphi \in U_{hc}^k. \tag{52}
\end{aligned}$$

Although this formulation is consistent - consistency results from the introduction of consistent fluxes -, the stability is not ensured. Indeed, linearization of formulation (52) leads to an expression similar to the one obtained for linear elasticity in [15] but for a quadratic term, which only appears in [15]. This quadratic term depends on a stabilization parameter  $\beta$  that has to be chosen large enough to lead to a stable weak statement of the problem. Therefore, after adding such a contribution, the final weak statement of the problem is finding  $\varphi_h \in U_h^k$  such that

$$\begin{aligned}
& \int_{\mathcal{A}_h} \bar{j} \bar{\mathbf{n}}^\alpha(\varphi_h) \cdot \delta \varphi_{,\alpha} d\mathcal{A}_0 + \int_{\mathcal{A}_h} \bar{j} \bar{\mathbf{m}}^\alpha(\varphi_h) \cdot (\delta \mathbf{t} \lambda_h)_{,\alpha} d\mathcal{A}_0 + \int_{\mathcal{A}_h} \bar{j} \bar{\mathbf{l}} \cdot \delta \mathbf{t} \lambda_h d\mathcal{A}_0 + \\
& \int_{\partial_I \mathcal{A}_h \cup \partial_T \mathcal{A}_h} \llbracket \delta \mathbf{t} \rrbracket \cdot \langle \bar{j} \lambda_h \bar{\mathbf{m}}^\alpha \rangle \nu_\alpha^- d\partial \mathcal{A}_0 + \int_{\partial_I \mathcal{A}_h \cup \partial_T \mathcal{A}_h} \llbracket \mathbf{t}(\varphi_h) \rrbracket \cdot \\
& \quad \langle \bar{j}_0 \mathcal{H}_m^{\alpha\beta\gamma\delta} (\delta \varphi_{,\gamma} \cdot \mathbf{t}_{,\delta} + \varphi_{,\gamma} \cdot \delta \mathbf{t}_{,\delta}) \varphi_{,\beta} + \bar{j} \lambda_h \bar{\mathbf{m}}^\alpha \cdot \varphi_{,\beta} \delta \varphi_{,\beta} \rangle \nu_\alpha^- d\partial \mathcal{A}_0 \\
& \quad \int_{\partial_I \mathcal{A}_h \cup \partial_T \mathcal{A}_h} \llbracket \mathbf{t}(\varphi_h) \rrbracket \cdot \varphi_{,\beta} \left\langle \frac{\beta \bar{j}_0 \mathcal{H}_m^{\alpha\beta\gamma\delta}}{h^s} \right\rangle \llbracket \delta \mathbf{t} \rrbracket \cdot \varphi_{,\gamma} \nu_\alpha^- \nu_\delta^- d\partial \mathcal{A}_0 \\
& = \int_{\partial_N \mathcal{A}_h} \bar{j} \bar{\mathbf{n}} \cdot \delta \varphi d\mathcal{A}_0 + \int_{\partial_M \mathcal{A}_h} \bar{j} \bar{\mathbf{m}} \cdot \delta \mathbf{t} \lambda_h d\mathcal{A}_0 + \\
& \quad \int_{\mathcal{A}_h} \mathbf{n}^{A_0} \cdot \delta \varphi \bar{j} d\mathcal{A}_0 + \int_{\mathcal{A}_h} \bar{\mathbf{m}}^{A_0} \cdot \delta \mathbf{t} \lambda_h \bar{j} d\mathcal{A}_0 \quad \forall \delta \varphi \in U_{hc}^k. \tag{53}
\end{aligned}$$

### 3.2. Numerical properties

Weak formulation (53) of the problem inherits consistency from its construction based on the use of consistent numerical fluxes (46). Indeed, if  $\varphi \in \mathbf{H}^4(\mathcal{A}_h)$  is the exact solution of the physical problem, it belongs to  $\mathcal{C}^2(\mathcal{A}_h)$ , which implies, via (7), that  $[[\mathbf{t}]] = 0$  on  $\partial_I \mathcal{A}_0$ , as opposed to  $[[\delta \mathbf{t}]]$ , and so for  $\mathbf{t}_{,\alpha}$  and  $\bar{j}$ . On the external boundary  $\partial_T \mathcal{A}_0$ ,  $[[\mathbf{t}]] = \bar{\mathbf{t}} - \mathbf{t} = 0$  and  $[[\delta \mathbf{t}]] = -\delta \mathbf{t}$ . Moreover, the resultant stress vectors  $\mathbf{n}^\alpha$  and  $\mathbf{m}^\alpha$ , as well as the thickness ratio  $\lambda_h$  of the exact solution are continuous across inter-element boundaries, which allows to rewrite the weak form (53) as

$$\begin{aligned} & \int_{\mathcal{A}_h} \bar{j} \mathbf{n}^\alpha \cdot \delta \varphi_{,\alpha} d\mathcal{A}_0 + \int_{\mathcal{A}_h} \bar{j} \tilde{\mathbf{m}}^\alpha \cdot (\delta \mathbf{t} \lambda_h)_{,\alpha} d\mathcal{A}_0 + \int_{\mathcal{A}_h} \bar{j} \mathbf{l} \cdot \delta \mathbf{t} \lambda_h d\mathcal{A}_0 + \\ & \int_{\partial_I \mathcal{A}_h \cup \partial_T \mathcal{A}_h} [[\delta \mathbf{t}]] \cdot \bar{j} \lambda_h \tilde{\mathbf{m}}^\alpha \nu_\alpha^- d\partial \mathcal{A}_0 = \int_{\partial_N \mathcal{A}_h} \bar{j} \bar{\mathbf{n}} \cdot \delta \varphi d\mathcal{A}_0 + \int_{\partial_M \mathcal{A}_h} \bar{j} \tilde{\mathbf{m}} \cdot \delta \mathbf{t} \lambda_h d\mathcal{A}_0 + \\ & \int_{\mathcal{A}_h} \mathbf{n}^{A_0} \cdot \delta \varphi \bar{j} d\mathcal{A}_0 + \int_{\mathcal{A}_h} \tilde{\mathbf{m}}^{A_0} \cdot \delta \mathbf{t} \lambda_h \bar{j} d\mathcal{A}_0 \quad \forall \delta \varphi \in \mathbf{U}_{hc}^k. \end{aligned} \quad (54)$$

After integration by parts, on each element  $\mathcal{A}_e$ , of the two first terms, this expression develops as

$$\begin{aligned} & \int_{\partial_N \mathcal{A}_h} \bar{j} \mathbf{n}^\alpha \cdot \delta \varphi \nu_\alpha d\partial \mathcal{A}_0 - \int_{\partial_I \mathcal{A}_h \cup \partial_T \mathcal{A}_h} \bar{j} \mathbf{n}^\alpha \cdot [[\delta \varphi]] \nu_\alpha^- d\partial \mathcal{A}_0 - \int_{\mathcal{A}_h} (\bar{j} \mathbf{n}^\alpha)_{,\alpha} \cdot \delta \varphi d\mathcal{A}_0 + \\ & \int_{\partial_M \mathcal{A}_h} \bar{j} \tilde{\mathbf{m}}^\alpha \cdot \delta \mathbf{t} \lambda_h \nu_\alpha d\partial \mathcal{A}_0 - \int_{\partial_I \mathcal{A}_h \cup \partial_T \mathcal{A}_h} \bar{j} \tilde{\mathbf{m}}^\alpha \cdot [[\delta \mathbf{t}]] \lambda_h \nu_\alpha^- d\partial \mathcal{A}_0 - \\ & \int_{\mathcal{A}_h} (\bar{j} \tilde{\mathbf{m}}^\alpha)_{,\alpha} \cdot \delta \mathbf{t} \lambda_h d\mathcal{A}_0 + \int_{\mathcal{A}_h} \bar{j} \mathbf{l} \cdot \delta \mathbf{t} \lambda_h d\mathcal{A}_0 + \int_{\partial_I \mathcal{A}_h \cup \partial_T \mathcal{A}_h} [[\delta \mathbf{t}]] \cdot \bar{j} \lambda_h \tilde{\mathbf{m}}^\alpha \nu_\alpha^- d\partial \mathcal{A}_0 = \\ & \int_{\partial_N \mathcal{A}_h} \bar{j} \bar{\mathbf{n}} \cdot \delta \varphi d\mathcal{A}_0 + \int_{\partial_M \mathcal{A}_h} \bar{j} \tilde{\mathbf{m}} \cdot \delta \mathbf{t} \lambda_h d\mathcal{A}_0 + \\ & \int_{\mathcal{A}_h} \mathbf{n}^{A_0} \cdot \delta \varphi \bar{j} d\mathcal{A}_0 + \int_{\mathcal{A}_h} \tilde{\mathbf{m}}^{A_0} \cdot \delta \mathbf{t} \lambda_h \bar{j} d\mathcal{A}_0 \quad \forall \delta \varphi \in \mathbf{U}_{hc}^k, \end{aligned} \quad (55)$$

where the definition (33) has been used. Since  $[[\delta\varphi]] = 0$ , Eq. (55) corresponds to the weak form of the set of equations

$$(\bar{j}\mathbf{n}^\alpha)_{,\alpha} + \bar{j}\mathbf{n}^{\mathcal{A}_0} = 0 \quad \text{in } \mathcal{A}_h, \quad (56)$$

$$(\bar{j}\tilde{\mathbf{m}}^\alpha)_{,\alpha} - \bar{j}\bar{\mathbf{l}} + \bar{j}\tilde{\mathbf{m}}^{\mathcal{A}_0} = \lambda_1 \mathbf{t} \quad \text{in } \mathcal{A}_h, \quad (57)$$

$$\bar{\bar{\mathbf{m}}} = \mathbf{m}^\alpha \nu_\alpha + \lambda_2 \mathbf{t} \quad \text{on } \partial_M \mathcal{A}_h, \quad (58)$$

$$\bar{\bar{\mathbf{n}}} = \mathbf{n}^\alpha \nu_\alpha \quad \text{on } \partial_N \mathcal{A}_h, \quad (59)$$

which correspond respectively to the governing equations (12), (13), (17) and (19), up to undefined values  $\lambda_i$ . Consistency of the weak formulation (53) is then ensured in the non-linear range.

Unfortunately, demonstration of the stability and convergence rate requires a linearization of the equations. Indeed, the internal forces resulting from the use of the general constitutive behavior described in section 2.3, do not generally lead to stability. This behavior has been shown in [34] for solid mechanics (not related to DG methods or shell description). Therefore new algorithms defining new stress tensors have been developed in the last 15 years to address this issue, see [34–36] among others. These developments are beyond the scope of the present work, and it is assumed, as for solid elements, that if the linearized form is stable, the non-linear extension is stable enough to conduct simulations.

To demonstrate the stability of the linearized form, new definitions are introduced, see [23] for details. First, the gradient of the unit vector is decomposed into the mid-surface convected basis as

$$(\lambda_h \mathbf{t})_{,\alpha} = \lambda_\alpha^\mu \varphi_{,\mu} + \lambda_\alpha^3 \lambda_h \mathbf{t}. \quad (60)$$

Since  $\lambda_{h,\alpha}$  is neglected, and since  $\mathbf{t}_{,\alpha} \cdot \mathbf{t} = 0$ , this last relation can be simplified into

$$\mathbf{t}_{,\alpha} = \frac{\lambda_{\alpha}^{\mu}}{\lambda_h} \boldsymbol{\varphi}_{,\mu} \quad \text{and} \quad \lambda_{\alpha}^3 = 0. \quad (61)$$

Similarly, in order to define the stress components, the resultant stress vectors are decomposed in this mid-surface convected basis, as

$$\mathbf{n}^{\alpha} = n^{\alpha\beta} \boldsymbol{\varphi}_{,\beta} + q^{\alpha} \lambda_h \mathbf{t}, \quad (62)$$

$$\tilde{\mathbf{m}}^{\alpha} = \tilde{m}^{\alpha\beta} \boldsymbol{\varphi}_{,\beta} + \tilde{m}^{3\alpha} \lambda_h \mathbf{t}, \quad \text{and} \quad (63)$$

$$\mathbf{l} = l^{\alpha} \boldsymbol{\varphi}_{,\alpha} + l^3 \lambda_h \mathbf{t}. \quad (64)$$

At this stage,  $n^{\alpha\beta}$  and  $q^{\alpha}$  are still coupled with the bending of the shell [17]. However, since  $\boldsymbol{\sigma}$  is symmetric, expression (103) established in appendix I, which is

$$\mathbf{n}^{\alpha} \wedge \boldsymbol{\varphi}_{,\alpha} + \tilde{\mathbf{m}}^{\alpha} \wedge (\lambda_h \mathbf{t})_{,\alpha} + \mathbf{l} \wedge \lambda_h \mathbf{t} = 0, \quad (65)$$

holds, and can be satisfied by enforcing the symmetry of the effective membrane stress resultant tensor, *i.e.*:

$$\tilde{n}^{\alpha\beta} \boldsymbol{\varphi}_{,\alpha} \otimes \boldsymbol{\varphi}_{,\beta} = \mathbf{n}^{\alpha} \otimes \boldsymbol{\varphi}_{,\alpha} + \mathbf{l} \otimes \lambda_h \mathbf{t} - (\lambda_h \mathbf{t})_{,\alpha} \otimes \tilde{\mathbf{m}}^{\alpha} = \tilde{n}^{\alpha\beta} \boldsymbol{\varphi}_{,\beta} \otimes \boldsymbol{\varphi}_{,\alpha}. \quad (66)$$

From (61) and (66), effective membrane stress resultant  $\tilde{n}^{ij}$  can be obtained by

$$\tilde{n}^{\alpha\beta} = n^{\alpha\beta} - \lambda_{\mu}^{\beta} \tilde{m}^{\alpha\mu} = \tilde{n}^{\beta\alpha}, \quad (67)$$

$$\tilde{n}^{3\alpha} = q^{\alpha} - \lambda_{\mu}^3 \tilde{m}^{\alpha\mu} = \tilde{q}^{\alpha}, \quad (68)$$

$$\tilde{n}^{\alpha 3} = l^{\alpha} - \lambda_{\mu}^{\alpha} \tilde{m}^{3\mu} = \tilde{l}^{\alpha} = \tilde{q}^{\alpha}, \quad \text{and by} \quad (69)$$

$$\tilde{n}^{33} = l^3 - \lambda_{\mu}^3 \tilde{m}^{3\mu} = \tilde{l}^3, \quad (70)$$

which are respectively the membrane effective stresses, effective transverse shear, effective symmetric shear and effective across-the-thickness stress.

Since plane stress is assumed, since Kirchhoff-Love shells are considered, and since the shearing resulting from  $\lambda_{h,\alpha}$  is neglected, the set of Eqs. (27-29) holds and

$$\tilde{n}^{3\alpha} = \tilde{q}^\alpha = \tilde{l}^\alpha = \tilde{n}^{33} = \tilde{l}^3 = 0. \quad (71)$$

Remaining components for a linear material are written, see [23], as

$$\tilde{n}^{\alpha\beta} = \frac{E(h_{\max} - h_{\min})\bar{j}_0}{(1 + \nu)\bar{j}} \left[ \left( \frac{\nu}{1 - 2\nu} \varphi_0^\alpha \cdot \varphi_0^\beta \varphi_0^\gamma \cdot \varphi_0^\delta + \frac{1}{2} \varphi_0^\alpha \cdot \varphi_0^\gamma \varphi_0^\beta \cdot \varphi_0^\delta + \right. \right. \\ \left. \left. \frac{1}{2} \varphi_0^\alpha \cdot \varphi_0^\delta \varphi_0^\beta \cdot \varphi_0^\gamma \right) \left( \frac{1}{2} \varphi_{0,\gamma} \cdot \varphi_{0,\delta} - \frac{1}{2} \varphi_{0,\gamma} \cdot \varphi_{0,\delta} \right) + \frac{\nu}{1 - 2\nu} \varphi_0^\alpha \cdot \varphi_0^\beta \varepsilon_{33} \right], \quad (72)$$

$$\tilde{m}^{\alpha\beta} = \frac{\bar{j}_0}{\lambda_{h,j}} \mathcal{H}_m^{\alpha\beta\gamma\delta} (\varphi_{0,\gamma} \cdot \mathbf{t}_{0,\delta} - \varphi_{0,\gamma} \cdot \mathbf{t}_{0,\delta}). \quad (73)$$

Deformation  $\varepsilon_{33}$  is computed from the plane stress assumption, and corresponds to  $\varepsilon_{33} = -\frac{\nu}{1-\nu} \varphi_0^\alpha \cdot \varphi_0^\beta \left( \frac{1}{2} \varphi_{0,\gamma} \cdot \varphi_{0,\delta} - \frac{1}{2} \varphi_{0,\gamma} \cdot \varphi_{0,\delta} \right)$ , which allows to simplify expressions (72-73) into

$$\tilde{n}^{\alpha\beta} = \frac{\bar{j}_0}{\bar{j}} \mathcal{H}_n^{\alpha\beta\gamma\delta} \left( \frac{1}{2} \varphi_{0,\gamma} \cdot \varphi_{0,\delta} - \frac{1}{2} \varphi_{0,\gamma} \cdot \varphi_{0,\delta} \right), \quad (74)$$

$$\tilde{m}^{\alpha\beta} = \frac{\bar{j}_0}{\lambda_{h,j}} \mathcal{H}_m^{\alpha\beta\gamma\delta} (\varphi_{0,\gamma} \cdot \mathbf{t}_{0,\delta} - \varphi_{0,\gamma} \cdot \mathbf{t}_{0,\delta}), \quad (75)$$

where

$$\mathcal{H}_n^{\alpha\beta\gamma\delta} = \frac{E(h_{\max} - h_{\min})}{(1 - \nu^2)} \left[ \nu \varphi_0^\alpha \cdot \varphi_0^\beta \varphi_0^\gamma \cdot \varphi_0^\delta + \frac{1}{2} (1 - \nu) \varphi_0^\alpha \cdot \varphi_0^\gamma \varphi_0^\beta \cdot \varphi_0^\delta + \right. \\ \left. \frac{1}{2} (1 - \nu) \varphi_0^\alpha \cdot \varphi_0^\delta \varphi_0^\beta \cdot \varphi_0^\gamma \right] \quad (76)$$

and where  $\mathcal{H}_m^{\alpha\beta\gamma\delta}$  is defined by (51).

All the terms of the weak form (53) can be rewritten after using Eqs. (61 -76), assuming small displacements

$$\varphi_h = \varphi_0 + \mathbf{u}_h, \quad (77)$$

and neglecting all quadratic terms. It successively yields

$$\begin{aligned}
\int_{\mathcal{A}_h} \bar{j} \mathbf{n}^\alpha \cdot \delta \varphi_{,\alpha} d\mathcal{A}_0 &= \int_{\mathcal{A}_h} \bar{j} \tilde{\mathbf{n}}^{\alpha\beta} \varphi_{0,\beta} \cdot \delta \mathbf{u}_{,\alpha} d\mathcal{A}_0 + \int_{\mathcal{A}_h} \bar{j} \tilde{\mathbf{m}}^{\alpha\mu} \lambda_\mu^\beta \varphi_{0,\beta} \cdot \delta \mathbf{u}_{,\alpha} d\mathcal{A}_0 \\
&= \int_{\mathcal{A}_h} \bar{j} \tilde{\mathbf{n}}^{\alpha\beta} \varphi_{0,\beta} \cdot \delta \mathbf{u}_{,\alpha} d\mathcal{A}_0 + \int_{\mathcal{A}_h} \bar{j} \tilde{\mathbf{m}}^{\alpha\beta} \lambda_h \mathbf{t}_{0,\beta} \cdot \delta \mathbf{u}_{,\alpha} d\mathcal{A}_0 \\
&= \int_{\mathcal{A}_h} \bar{j}_0 \frac{1}{4} (\varphi_{0,\gamma} \cdot \mathbf{u}_{h,\delta} + \varphi_{0,\delta} \cdot \mathbf{u}_{h,\gamma}) \mathcal{H}_n^{\alpha\beta\gamma\delta} (\varphi_{0,\beta} \delta \mathbf{u}_{,\alpha} + \varphi_{0,\alpha} \delta \mathbf{u}_{,\beta}) d\mathcal{A}_0 \\
&\quad + \int_{\mathcal{A}_h} \bar{j}_0 (\mathbf{u}_{h,\gamma} \cdot \mathbf{t}_{0,\delta} + \varphi_{0,\gamma} \cdot \Delta \mathbf{t}_{,\delta}) \mathcal{H}_m^{\alpha\beta\gamma\delta} \mathbf{t}_{0,\beta} \cdot \delta \mathbf{u}_{,\alpha} d\mathcal{A}_0, \quad (78)
\end{aligned}$$

$$\begin{aligned}
\int_{\mathcal{A}_h} \bar{j} \tilde{\mathbf{m}}^\alpha \cdot (\delta \mathbf{t} \lambda_h)_{,\alpha} d\mathcal{A}_0 &= \int_{\mathcal{A}_h} \bar{j} \lambda_h \tilde{\mathbf{m}}^{\alpha\beta} \varphi_{0,\beta} \cdot \delta \mathbf{t}_{,\alpha} d\mathcal{A}_0 \\
&= \int_{\mathcal{A}_h} \bar{j}_0 (\mathbf{u}_{h,\gamma} \cdot \mathbf{t}_{0,\delta} + \varphi_{0,\gamma} \cdot \Delta \mathbf{t}_{,\delta}) \mathcal{H}_m^{\alpha\beta\gamma\delta} \varphi_{0,\beta} \cdot \delta \Delta \mathbf{t}_{,\alpha} d\mathcal{A}_0, \quad (79)
\end{aligned}$$

$$\begin{aligned}
\int_{\partial_I \mathcal{A}_h \cup \partial_T \mathcal{A}_h} [[\delta \mathbf{t}]] \cdot \langle \bar{j} \lambda_h \tilde{\mathbf{m}}^\alpha \rangle \nu_\alpha^- d\partial \mathcal{A}_0 &= \int_{\partial_I \mathcal{A}_h \cup \partial_T \mathcal{A}_h} [[\delta \Delta \mathbf{t}]] \cdot \langle \bar{j} \lambda_h \tilde{\mathbf{m}}^{\alpha\beta} \varphi_{0,\beta} \rangle \nu_\alpha^- d\partial \mathcal{A}_0 = \\
\int_{\partial_I \mathcal{A}_h \cup \partial_T \mathcal{A}_h} [[\delta \Delta \mathbf{t}]] \cdot \langle \bar{j}_0 \mathcal{H}_m^{\alpha\beta\gamma\delta} (\mathbf{u}_{h,\gamma} \cdot \mathbf{t}_{0,\delta} + \varphi_{0,\gamma} \cdot \Delta \mathbf{t}_{,\delta}) \varphi_{0,\beta} \rangle \nu_\alpha^- d\partial \mathcal{A}_0, \quad (80)
\end{aligned}$$

$$\begin{aligned}
\int_{\partial_I \mathcal{A}_h \cup \partial_T \mathcal{A}_h} [[\mathbf{t}]] \cdot \langle \bar{j}_0 \mathcal{H}_m^{\alpha\beta\gamma\delta} (\delta \varphi_{,\gamma} \cdot \mathbf{t}_{,\delta} + \varphi_{,\gamma} \cdot \delta \mathbf{t}_{,\delta}) \varphi_{,\beta} + \bar{j} \lambda_h \tilde{\mathbf{m}}^\alpha \cdot \varphi_{,\beta} \delta \varphi_{,\beta} \rangle \nu_\alpha^- d\partial \mathcal{A}_0 \\
= \int_{\partial_I \mathcal{A}_h \cup \partial_T \mathcal{A}_h} [[\Delta \mathbf{t}]] \cdot \langle \bar{j}_0 \mathcal{H}_m^{\alpha\beta\gamma\delta} (\delta \mathbf{u}_{,\gamma} \cdot \mathbf{t}_{0,\delta} + \varphi_{0,\gamma} \cdot \delta \Delta \mathbf{t}_{,\delta}) \varphi_{0,\beta} \rangle \nu_\alpha^- d\partial \mathcal{A}_0, \text{ and to } \quad (81)
\end{aligned}$$

$$\begin{aligned}
\int_{\partial_I \mathcal{A}_h \cup \partial_T \mathcal{A}_h} [[\mathbf{t}]] \cdot \varphi_{,\beta} \left\langle \frac{\beta \bar{j}_0 \mathcal{H}_m^{\alpha\beta\gamma\delta}}{h^s} \right\rangle [[\delta \mathbf{t}]] \cdot \varphi_{,\gamma} \nu_\alpha^- \nu_\delta^- d\partial \mathcal{A}_0 = \\
\int_{\partial_I \mathcal{A}_h \cup \partial_T \mathcal{A}_h} [[\Delta \mathbf{t}]] \cdot \varphi_{0,\beta} \left\langle \frac{\beta \bar{j}_0 \mathcal{H}_m^{\alpha\beta\gamma\delta}}{h^s} \right\rangle [[\delta \Delta \mathbf{t}]] \cdot \varphi_{0,\gamma} \nu_\alpha^- \nu_\delta^- d\partial \mathcal{A}_0, \quad (82)
\end{aligned}$$

where  $\Delta \mathbf{t} = \mathbf{t} - \mathbf{t}_0$ . Using these last relations, the weak formulation (53) can be linearized to a bilinear form, which is finding  $\mathbf{u}_h \in \mathbf{U}_h^k$  such that

$$a(\mathbf{u}_h, \delta \mathbf{u}) = b(\delta \mathbf{u}) \quad \forall \delta \mathbf{u} \in \mathbf{U}_{hc}^k, \quad (83)$$

where

$$\begin{aligned}
a(\mathbf{u}_h, \delta \mathbf{u}) = & \int_{\mathcal{A}_h} \left( \frac{1}{2} \boldsymbol{\varphi}_{0,\gamma} \cdot \mathbf{u}_{h,\delta} + \frac{1}{2} \mathbf{u}_{h,\gamma} \cdot \boldsymbol{\varphi}_{0,\delta} \right) \mathcal{H}_n^{\alpha\beta\gamma\delta} \left( \frac{1}{2} \boldsymbol{\varphi}_{0,\alpha} \cdot \delta \mathbf{u}_{,\beta} + \frac{1}{2} \boldsymbol{\varphi}_{0,\beta} \cdot \delta \mathbf{u}_{,\alpha} \right) \bar{j}_0 d\mathcal{A}_0 + \\
& \int_{\mathcal{A}_h} \left( \boldsymbol{\varphi}_{0,\gamma} \cdot \boldsymbol{\Delta} \mathbf{t}(\mathbf{u}_h)_{,\delta} + \mathbf{u}_{h,\gamma} \cdot \mathbf{t}_{0,\delta} \right) \mathcal{H}_m^{\alpha\beta\gamma\delta} \left( \boldsymbol{\varphi}_{0,\alpha} \cdot \delta \boldsymbol{\Delta} \mathbf{t}(\mathbf{u})_{,\beta} + \delta \mathbf{u}_{,\alpha} \cdot \mathbf{t}_{0,\beta} \right) \bar{j}_0 d\mathcal{A}_0 + \\
& \int_{\partial_I \mathcal{A}_h \cup \partial \mathcal{A}_h} \llbracket \boldsymbol{\Delta} \mathbf{t}(\mathbf{u}_h) \rrbracket \cdot \left\langle \boldsymbol{\varphi}_{0,\gamma} \mathcal{H}_m^{\alpha\beta\gamma\delta} \left( \boldsymbol{\varphi}_{0,\alpha} \cdot \delta \boldsymbol{\Delta} \mathbf{t}(\mathbf{u})_{,\beta} + \delta \mathbf{u}_{,\alpha} \cdot \mathbf{t}_{0,\beta} \right) \bar{j}_0 \right\rangle \nu_{\delta}^{-} d\partial \mathcal{A}_0 + \\
& \int_{\partial_I \mathcal{A}_h \cup \partial \mathcal{A}_h} \llbracket \delta \boldsymbol{\Delta} \mathbf{t}(\mathbf{u}) \rrbracket \cdot \left\langle \boldsymbol{\varphi}_{0,\gamma} \mathcal{H}_m^{\alpha\beta\gamma\delta} \left( \boldsymbol{\varphi}_{0,\alpha} \cdot \boldsymbol{\Delta} \mathbf{t}(\mathbf{u}_h)_{,\beta} + \mathbf{u}_{h,\alpha} \cdot \mathbf{t}_{0,\beta} \right) \bar{j}_0 \right\rangle \nu_{\delta}^{-} d\partial \mathcal{A}_0 + \\
& \int_{\partial_I \mathcal{A}_h \cup \partial \mathcal{A}_h} \frac{\beta}{h^s} \llbracket \delta \boldsymbol{\Delta} \mathbf{t} \rrbracket \cdot \boldsymbol{\varphi}_{0,\gamma} \nu_{\delta}^{-} \left\langle \mathcal{H}_m^{\alpha\beta\gamma\delta} \bar{j}_0 \right\rangle \llbracket \boldsymbol{\Delta} \mathbf{t}(\mathbf{u}_h) \rrbracket \cdot \boldsymbol{\varphi}_{0,\alpha} \nu_{\beta}^{-} d\partial \mathcal{A}_0, \tag{84}
\end{aligned}$$

and where

$$\begin{aligned}
b(\delta \mathbf{u}) = & \int_{\mathcal{A}_h} (\mathbf{n}^{A_0} \cdot \delta \mathbf{u} + \bar{\mathbf{m}}^{A_0} \cdot \delta \boldsymbol{\Delta} \mathbf{t}) \bar{j}_0 d\mathcal{A}_0 + \\
& \int_{\partial_N \mathcal{A}_h} \bar{\mathbf{n}} \cdot \delta \mathbf{u} \bar{j}_0 d\partial \mathcal{A}_0 + \int_{\partial_M \mathcal{A}_0} \bar{\mathbf{m}} \cdot \delta \boldsymbol{\Delta} \mathbf{t} \bar{j}_0 d\partial \mathcal{A}_0, \tag{85}
\end{aligned}$$

which corresponds to the formulation proposed for linear elasticity in [15]. Although in this work symmetry and stability terms have been added to the weak form, leading to an interior penalty method, which prevents the formulation of being derived from a functional as it is the case with linear shells [15], it is worth noticing that the linearized forms correspond to each other. The present formulation inherits therefore, in the linear range, the properties of the former. In particular, stability is ensured if the stability parameter  $\beta$  is larger than a constant depending on the polynomial approximation  $k$ , and on the element shape. Assuming the exact solution belongs to  $\mathbf{H}^{k+1}$ , the convergence rate of the method in the energy norm, with respect to the mesh-size, is equal to  $k-1$ , which justifies the use of quadratic or higher order elements. Under the same assumption, the convergence rate in the  $L^2$ -norm, is equal to  $k+1$  if  $k > 2$  and is quadratic for quadratic elements.

In the non-linear range, these properties are also expected. Let us note that the somehow artificial introduction of symmetry and stability terms, based on a constant Hooke tensor, is justified by the fact these terms cannot vanish with non-linear materials (*e.g.* perfectly plastic materials), which could be the case when using lifting operators as it was discussed in [9].

Similar results have also been obtained for linear Kirchhoff plates, see [10, 12].

As it is shown in the following section, these properties are still observed on numerical examples involving large deformations, but they cannot be demonstrated.

#### 4. NUMERICAL APPLICATIONS

The discontinuous Galerkin formulation presented in section 3 is implemented by recourse to interface elements. These interface elements are inserted between two adjacent shell elements and integrate the 3 interface contributions. Implementation of this interface element closely follows the one described for linear elasticity [15] and is not repeated here.

In particular, two kinds of elements are considered:

- 9-node bi-quadratic quadrangles with 4-Gauss-point reduced integration;
- 16-node bi-cubic quadrangles with 16-Gauss-point full integration.

Indeed, if quadratic elements require EAS or reduced integration to avoid locking, cubic elements do not suffer from this limitation.

In this work, a neo-Hookean model is considered, with

$$W = \left( \frac{K_0}{2} - \frac{G_0}{3} \right) \log^2 J - G_0 \log J + \frac{G_0}{2} (\text{tr} \mathbf{C} - 3), \quad (86)$$

where  $K_0$  and  $G_0$  are respectively the bulk and shear moduli. Therefore, the components of

the Kirchhoff tensor (24) in the convected basis becomes

$$\tau^{ij} = \left( K_0 - \frac{2}{3}G_0 \right) \log J \mathbf{g}^i \cdot \mathbf{g}^j - G_0 \left( \mathbf{g}^i \cdot \mathbf{g}^j - \mathbf{g}_0^i \cdot \mathbf{g}_0^j \right). \quad (87)$$

The corresponding tangent moduli is written

$$\begin{aligned} C^{ijkl} = & \left( K_0 - \frac{2}{3}G_0 \right) \mathbf{g}^i \cdot \mathbf{g}^j \mathbf{g}^k \cdot \mathbf{g}^l - \\ & \left[ \left( K_0 - \frac{2}{3}G_0 \right) \log J - G_0 \right] \left( \mathbf{g}^i \cdot \mathbf{g}^k \mathbf{g}^j \cdot \mathbf{g}^l + \mathbf{g}^i \cdot \mathbf{g}^l \mathbf{g}^j \cdot \mathbf{g}^k \right). \end{aligned} \quad (88)$$

Finally, it is assumed that the forces are applied on the mid-surface of the shell, see [23] for discussion.

#### 4.1. Pinched open hemisphere

[Figure 2 about here.]

[Table 1 about here.]

This classical example, proposed in [37], consists into an open hemisphere, with radius  $R$ , thickness  $t$ , and an opening of a spherical sector angle  $\theta$ . It is subjected to radial loads  $P$  applied on two diametral directions, see Fig. 2a. The load is compressive in the  $y$ -direction and tensile in  $x$ -direction. One quarter of the structure is modeled exploiting the symmetries of the problem. Analytical deflection under the loads can be computed analytically for small deformations ( $|\delta_x| = |\delta_y| = 0.093 \text{ [m} \cdot \text{N}^{-1}] \frac{P}{2}$ ), while numerical tests have been performed for large deformations, see [24, 26, 27, 29–31, 33, e.g.] for the geometry reported in Table I. Among these references, 2 converged for the maximum loading or 800 N:

- The mixed Enhanced Assumed Strains formulation proposed by Bischoff and Ram [26] and applied to 4 and 9-node quadrangles. This formulation uses 6 degrees of freedom per

node (3 displacements, 2 rotations and the thickness).

- The mixed formulation based on mid-side rotations proposed by Areias *et al.* [33]. This formulation is based on the Kirchhoff-Love assumption as for the present formulation. The solution obtained by this method with 24 elements on each side is the reference used to assess the accuracy of the proposed DG method.

[Figure 3 about here.]

This simulation is computed using the proposed discontinuous Galerkin formulation with 9-node bi-quadratic and 16-node bi-cubic elements. Even if due to the hemispheric shape a regular mesh leads to distorted element, this aspect is emphasized by considering the so called distorted mesh. It consists into quadrangular elements with spacing between two nodes following a regular progression. So along curves parallel to plane  $xOy$ , 2 consecutive nodes near plane  $xOz$  are localized at a distance twice smaller than 2 consecutive nodes near plane  $yOz$ . Nodes on a meridian obey to a similarly distribution and 2 consecutive nodes near the  $18^\circ$  hole are localized at a distance twice smaller than 2 consecutive nodes near plane  $xOy$ . The purpose of such a mesh is to demonstrate that the method does not suffer from locking when elements are distorted. Final deformed configurations for regular and distorted cubic elements are shown in Figure 2b and c respectively, while the displacement evolutions of nodes A and B in terms of the applied load are illustrated on Figure 3. It can be seen that the method always converges for the maximum loading, and that it does not suffer from locking even with a distorted mesh. On the contrary, since the mesh size is reduced near node A, which experiences the larger bending deformation, the distorted mesh leads to a better approximation of the solution. The results obtained with 8 cubic elements on each side are compared to results obtained with

12 quadratic elements on each side, which leads to the same number of node on an edge. It is observed than quadratic elements reach a slightly better approximation of the solution. Finally, it is observed, as expected, than, contrarily to linear elasticity, the displacements of node A and B are not equal, except in the range of small deformations ( $P < 10$  N).

[Figure 4 about here.]

[Figure 5 about here.]

Influences of the stabilization parameter and of the mesh size on the results are also studied. In order to ensure convergence of the simulations for a wide range of, not necessarily optimal, parameters, the loading considered is  $P = 400$  N, or half the previously used one, which still leads to large deformations and rotations. Figure 4a illustrates the displacements of point A and B for a stabilization parameter  $\beta$  belonging to the range  $[1; 10^4]$ , and for two different meshes; the first mesh has 8 bi-cubic quadrangles on each side, and the second mesh has 12 bi-cubic quadrangles on each side, which leads to the same number of nodes in both cases. As the linear theory is predicting it, see [15], the solution is stable only when  $\beta$  is larger than a polynomial-degree dependent constant. Indeed, as long as  $\beta$  is larger than 100 for quadratic elements and larger than 10 for cubic elements, the solution is stable and the influence of the stabilization parameter is limited to less than 1 %. As it is shown in Figure 4b, the mesh size dependency is more dramatic. During this study, two mesh evolutions are considered. First, 2, 4, 8, 16 and 20 bi-cubic and then 3, 6, 12 and 24 bi-quadratic elements on each side are successively used, and for a constant stabilization parameter  $\beta = 10^2$ . In both cases, if the coarsest meshes capture only 70% of the deformations, the solutions always convergence when the mesh size is reduced. Accordingly to the linear theory, the convergence rate in this  $L^2$ -norm

is one degree higher than the polynomial approximation for cubic elements and is quadratic for quadratic elements, as illustrated by Figure 5.

#### 4.2. Thin plate ring

[Figure 6 about here.]

[Table 2 about here.]

This example was first proposed in [24] and consists into a thin plate ring, with inner radius  $R_i$ , outer radius  $R_e$  and thickness  $t$ , with the geometry reported in Table II. This ring is cut along a radius AB, and, on one side of this cutting, the plate is clamped, while a uniform vertical loading  $q$  is applied on the other side, see Figure 6a. This test has widely been used in the literature, see [25, 28, 30, 33, e.g.] to compare shells formulations when large rotations arise.

[Figure 7 about here.]

This simulation is computed using the proposed discontinuous Galerkin formulation applied to 9-node bi-quadratic elements. The final deformed configuration is illustrated in Figure 6b, and the displacement evolutions of nodes A and B located at the cutting are shown in Figure 7. Although the mesh experiences large distortion during the deformation process, the solution is in good agreement with the ones obtained in the literature, and in particular with:

- The hybrid stress formulation proposed by Sansour and Kollmann [30], for whom results are displayed for  $q < 3000 \text{ N}\cdot\text{m}^{-1}$  (which the maximum loading considered in this reference).

- The mixed formulation based on mid-side rotations proposed by Areias *et al.* [33], which converges for an applied linear force reaching  $12000 \text{ N}\cdot\text{m}^{-1}$ .

#### 4.3. Clamped cylinder

[Figure 8 about here.]

[Table 3 about here.]

This example consisting into a thin cylinder, with radius  $R$ , length  $L$  and thickness  $t$ , clamped at one extremity and pinched at the other one by two diametral opposite forces  $P$  applied on point A, see Figure 8a. This test has been considered by several authors, see [31–33, e.g.], for the geometry reported in Table III. The solution obtained with the present formulation is compared to the computational results obtained in [31], with 5-degree of freedom per node linear shells, for a maximum loading of 1.6 kN.

[Figure 9 about here.]

Simulation was first conducted with 12 bi-quadratic quadrangles on each edge and for the stabilization  $\beta = 10^2$ . Deformations obtained for  $P = 400, 752, 800, 1200$  and  $1600 \text{ N}$ , are respectively reported in Figures 8b-f. Particularly, for  $P = 752 \text{ N}$  the two free edges of the cylinder enter into contact. Although, the remaining part of the simulation is no longer physical, it is usually conducted [31,33] in order to demonstrate the robustness of the method. Evolution of point A displacement with respect to the loading is shown in Figure 9 and is compared to a simulation using 8 bi-cubic quadrangles on each side, which leads to the same number of degrees of freedom. Both results are comparable to the reference [31], which demonstrates the accuracy of the new formulation and its ability to capture complex state of deformation.

## 5. CONCLUSIONS

A generalization to finite deformations of the discontinuous Galerkin formulation of linear Kirchhoff-Love shells presented previously in [15] has been developed.

Toward this end, the shell kinematics proposed by Simo *et al.* [23], which introduces the thickness ratio, is simplified by neglected geometrical shearing resulting from the misalignment of the shell section with the shell normal, but also by neglecting shearing resulting from the deformation gradient in the shell thickness. With these assumptions, the equations governing the shell motion can be stated in terms of the displacement field only.

The thickness stretch is computed by assuming a plane-stress state all along the shell thickness. Numerical integration of the resulting stress tensor on the thickness is achieved by recourse to a Simpson rule, and leads to the resultant membrane and bending stress vectors, which constitute the bases to establish the new weak formulation of the problem.

When establishing this weak form, the discontinuities in the displacement derivative between two elements are accounted for by considering the variation in their normal direction, leading to inter-element boundary terms in the resulting discontinuous Galerkin weak formulation of Kirchhoff-love shells.

After linearization of this new formulation, the set of equations reduces to the linear DG method developed in the linear range, in which case, it has been demonstrated that these interface terms ensure consistency, optimal convergence rate and stability of the method. In the non-linear range, only consistency can be rigorously demonstrated, but the other numerical properties are observed on numerical examples

Numerical examples, involving large deformations and large rotations are performed by considering 9-node, 4-Gauss-point bi-quadratic and 16-node, 16-Gauss-point bi-cubic

quadrangular shell elements. Agreement to results of the literature is excellent, and the method has been shown to converge for the most severe loading used for other shell formulations.

The one-field formulation presented herein is particularly appealing and should constitute a advantage as more complex material behaviors, involving plasticity, will be considered in the forthcoming works.

#### REFERENCES

1. F. Cirak, M. Ortiz, and P. Schröder. Subdivision surfaces: a new paradigm for thin-shell finite-element analysis. *International Journal for Numerical Methods in Engineering*, 47:2039–2072, 2000.
2. O.C. Zienkiewicz and R.L. Taylor. *The Finite Element method, 4th edn.* McGraw-Hill, New York, 1994.
3. F. Cirak and M. Ortiz. Fully  $C^1$ -conforming subdivision elements for finite deformation thin-shell analysis. *International Journal for Numerical Methods in Engineering*, 51:813–833, 2001.
4. A. Lew, P. Neff, D. Sulsky, and M. Ortiz. Optimal BV estimates for a discontinuous Galerkin method for linear elasticity. *Applied Mathematics Research eXpress*, 3:73–106, 2004.
5. A. Ten Eyck and A. Lew. Discontinuous Galerkin methods for non-linear elasticity. *International Journal for Numerical Methods in Engineering*, 67:1204–1243, 2006.
6. L. Noels and R. Radovitzky. A general discontinuous Galerkin method for finite hyperelasticity. Formulation and numerical applications. *International Journal for Numerical Methods in Engineering*, 68(1):64–97, 2006.
7. L. Noels and R. Radovitzky. Alternative approaches for the derivation of discontinuous Galerkin methods for nonlinear mechanics. *Journal of Applied Mechanics*, 74:1031–1045, 2007.
8. A. Ten Eyck, A. Celiker, and A. Lew. Adaptive stabilization of discontinuous galerkin methods for nonlinear elasticity: Motivation, formulation and numerical examples. *Computer Methods in Applied Mechanics and Engineering*, 197:–, 2008.
9. L. Noels and R. Radovitzky. An explicit discontinuous Galerkin method for non-linear solid dynamics. Formulation, parallel implementation and scalability properties. *International Journal for Numerical Methods in Engineering*, 74:1393–1420, 2008.
10. G Engel, K. Garikipati, T.J.R. Hughes, M.G. Larson, L Mazzei, and RL Taylor. Continuous/discontinuous

- finite element approximations of fourth-order elliptic problems in structural and continuum mechanics with applications to thin beams and plates. *Computer Methods in Applied Mechanics and Engineering*, 191:3669–3750, 2002.
11. P. Hansbo and M.G. Larson. A discontinuous Galerkin method for the plate equation. *CALCOLO*, 39:41–59, 2002.
  12. G.N. Wells and N.T. Dung. A  $C^0$  discontinuous Galerkin formulation for Kirchhoff plates. *Computer Methods in Applied Mechanics and Engineering*, 196:3370–3380, 2007.
  13. G.N. Wells, K. Garikipati, and L. Molari. A discontinuous Galerkin method for strain gradient-dependent damage. *Computer Methods in Applied Mechanics and Engineering*, 193:3633–3645, 2004.
  14. L. Molari, G.N. Wells, K. Garikipati, and F. Ubertini. A discontinuous Galerkin method for strain gradient-dependent damage: Study of interpolations and convergence. *Computer Methods in Applied Mechanics and Engineering*, 195:1480–1498, 2006.
  15. L. Noels and R. Radovitzky. A new discontinuous Galerkin method for kirchhoff-love shells. *Computer Methods in Applied Mechanics and Engineering*, 197:2901–2929, 2008.
  16. N. Dung and G. Wells. Geometrically nonlinear formulation for thin shells without rotation degrees of freedom. *Computer Methods in Applied Mechanics and Engineering*, 197:2778–2788, 2008.
  17. J.C. Simo and D.D. Fox. On a stress resultant geometrically exact shell model. Part I: formulation and optimal parametrization. *Computer Methods in Applied Mechanics and Engineering*, 72:267–304, 1989.
  18. J.C. Simo, D.D. Fox, and M.S. Rifai. On a stress resultant geometrically exact shell model. Part II: the linear theory; computational aspects. *Computer Methods in Applied Mechanics and Engineering*, 73:53–92, 1989.
  19. T. Belytschko and I. Leviathan. Physical stabilization of the 4-node shell element with one point quadrature. *Computer Methods in Applied Mechanics and Engineering*, 113:321–350, 1994.
  20. Q. Zeng and A. Combescure. A new one-point quadrature, general non-linear quadrilateral shell element with physical stabilization. *International Journal for Numerical Methods in Engineering*, 42:1307–1338, 1998.
  21. K.J. Bathe and N. Dvorkin. A four-node plate bending element based on Mindlin/Reissner plate theory and a mixed interpolation. *International Journal for Numerical Methods in Engineering*, 21:367–383, 1985.
  22. K.J. Bathe and N. Dvorkin. A formulation of general shell elements - the use of mixed interpolation of tensorial components. *International Journal for Numerical Methods in Engineering*, 22:697–722, 1986.

23. J.C. Simo, D.D. Fox, and M.S. Rifai. On a stress resultant geometrically exact shell model. Part IV: variable thickness shells with through-the-thickness stretching. *Computer Methods in Applied Mechanics and Engineering*, 81:91–126, 1990.
24. Y. Basar and Y. Ding. Finite-rotation shell elements for the analysis of finite-rotation shell problems. *International Journal for Numerical Methods in Engineering*, 34:165–169, 1992.
25. N. Buechter and R. Ekkerhard. Shell theory versus degeneration – A comparison in large rotation finite element analysis. *International Journal for Numerical Methods in Engineering*, 34:39–59, 1992.
26. M. Bischoff and E. Ramm. Shear deformable shemm elements for large strains and rotations. *International Journal of Plasticity*, 40:4427–4449, 1997.
27. P. Betsch, A. Menzel, and A. Stein. On parametrization of finite rotations in computational mechanics. a classification of concepts with application to smooth shells. *Computer Methods in Applied Mechanics and Engineering*, 155:273–305, 1998.
28. C. Sansour and J. Bocko. On hybrid stress, hybrid strain and enhanced strain finite element formulations for a geometrically exact shell theory with drilling degrees of freedom. *International Journal for Numerical Methods in Engineering*, 43:175–192, 1998.
29. M. Li and F. Zhan. The finite deformation theory for beam, plate and shell. Part V: The shell element with drilling degree of freedom based on biot strain. *Computer Methods in Applied Mechanics and Engineering*, 189:743–759, 2000.
30. C. Sansour and F.G. Kollman. Families of 4-node and 9-node finite elements for a finite deformation shell theory. An assessment of hybrid stress, hybrid strain and enhanced strain elements. *Computational Mechanics*, 24:435–447, 2000.
31. A. Ibrahimbegović, B. Brank, and P. Courtois. Stress resultant geometrically exact form of classical shell model and vector-like parameterization of constrained finite rotations. *International Journal for Numerical Methods in Engineering*, 52:1235–1252, 2001.
32. A. Eriksson and Pacoste C. Element formulation and numerical techniques for stability problems in shells. *Computer Methods in Applied Mechanics and Engineering*, 191:3375–3810, 2002.
33. P.M.A. Areias, J.-H. Song, and T. Belytschko. A finite strain quadrilateral shell element based on discrete kirchhoff-love constraints. *International Journal for Numerical Methods in Engineering*, 64:1166–1206, 2005.
34. JC Simo and N Tarnow. The discrete energy-momentum method. Conserving algorithms for nonlinear elastodynamics. *ZAMP*, 43:757–792, 1992.

35. JC Simo and O Gonzalez. Recent results on the numerical integration of infinite-dimensional hamiltonian system. In TJR Hughes, E Onate, and OC Zienkiewicz, editors, *Recent Developments in Finite Element Analysis*, pages 255–271, CIMNE, Barcelona, Spain, 1994.
36. O Gonzalez. Exact energy and momentum conserving algorithms for general models in nonlinear elasticity. *Computer Methods in Applied Mechanics and Engineering*, 190:1763–1783, 2000.
37. R.H. MacNeal and R.L. Harder. A proposed standard set of problems to test finite element accuracy. *Finite Elements in Analysis and Design*, 1(1):3–20, 1985.

## APPENDIX

## I. THE MOMENTUM EQUATIONS

The resultant form of the momentum equations are established following argumentation in [17], but, in section changes in the shell thickness are considered.

Toward this end, the local linear momentum equation

$$\nabla \cdot \boldsymbol{\sigma} + \mathbf{B} = 0 \quad \text{in } \mathcal{S} \quad (89)$$

is integrated on the current configuration of the shell  $\mathcal{S}$ , leading, after using the divergence theorem, to

$$\int_{\partial \mathcal{S}} \boldsymbol{\sigma} \hat{\mathbf{n}} \, d\partial \mathcal{S} + \int_{\mathcal{S}} \mathbf{B} \, d\mathcal{S} = 0, \quad (90)$$

where  $\hat{\mathbf{n}}$  is the normal of the body in the current configuration. Nanson formula, which reads  $\hat{\mathbf{n}} d\partial \mathcal{S} = j [\nabla \Phi]^{-T} \hat{\mathbf{N}} d\Gamma$ , where  $\Gamma$  is the boundary of  $\mathcal{A}_0 \times [h_{\min 0}; h_{\max 0}]$ , and  $\hat{\mathbf{N}}$  its outer normal, allows to rewrite (90) as

$$\int_{\partial(\mathcal{A}_0 \times [h_{\min 0}; h_{\max 0}])} j \boldsymbol{\sigma} [\nabla \Phi]^{-T} \hat{\mathbf{N}} \, d\partial \Gamma + \int_{\mathcal{A}_0 \times [h_{\min 0}; h_{\max 0}]} \frac{\rho_0}{\rho} \mathbf{B} \, d\mathcal{A}_0 \, d\xi = 0. \quad (91)$$

Since  $\hat{\mathbf{N}} = \boldsymbol{\nu}$  on the lateral surfaces and  $\hat{\mathbf{N}} = \pm E^3$  on the top and bottom surfaces, this last relation becomes

$$\int_{\partial \mathcal{A}_0} \int_{h_{\min 0}}^{h_{\max 0}} j \boldsymbol{\sigma} \mathbf{g}^\alpha \, d\xi^3 \nu_\alpha \, d\partial \mathcal{A}_0 + \int_{\mathcal{A}_0} [j \boldsymbol{\sigma} \mathbf{g}^3]_{h_{\min 0}}^{h_{\max 0}} \, d\mathcal{A}_0 + \int_{\mathcal{A}_0 \times [h_{\min 0}; h_{\max 0}]} \frac{\rho_0}{\rho} \mathbf{B} \, d\mathcal{A}_0 \, d\xi = 0. \quad (92)$$

Using definitions (9) and (14), and applying Gauss theorem, the resulting form of the linear momentum equation becomes

$$\int_{\partial \mathcal{A}_0} \left[ (\bar{j} \mathbf{n}^\alpha)_{,\alpha} + \bar{j} \mathbf{n}^{\mathcal{A}_0} \right] \, d\mathcal{A}_0 = 0, \quad (93)$$

which, owing to the arbitrary choice of  $\mathcal{A}_0^\dagger$  leads to

$$\frac{1}{\bar{j}} (\bar{j} \mathbf{n}^\alpha)_{,\alpha} + \mathbf{n}^{\mathcal{A}_0} = 0 \quad \text{on } \mathcal{A}_0. \quad (94)$$

The same technique is used on the local angular momentum equation

$$\Phi \wedge \nabla \cdot \sigma + \Phi \wedge \mathbf{B} = 0 \quad \text{in } \mathcal{S}, \quad (95)$$

which is also integrated on the current configuration of the shell  $\mathcal{S}$ , leading to

$$\int_{\mathcal{S}} \Phi \wedge (\nabla \cdot \sigma) \, d\partial\mathcal{S} + \int_{\mathcal{S}} \Phi \wedge \mathbf{B} \, d\mathcal{S} = 0, \quad (96)$$

which becomes, after applying divergence theorem, and if  $e_{ijk}$  is the permutation tensor:

$$\begin{aligned} 0 &= \int_{\mathcal{S}} e_{ijk} \Phi_j \nabla_l \sigma_{kl} \, d\partial\mathcal{S} + \int_{\mathcal{S}} \Phi \wedge \mathbf{B} \, d\mathcal{S} \\ &= \int_{\mathcal{S}} e_{ijk} \nabla_l (\Phi_j \sigma_{kl}) \, d\partial\mathcal{S} - \int_{\mathcal{S}} \nabla_l \Phi_j e_{ijk} \sigma_{kl} \, d\partial\mathcal{S} + \int_{\mathcal{S}} \Phi \wedge \mathbf{B} \, d\mathcal{S} \\ &= \int_{\partial\mathcal{S}} \Phi \wedge (\sigma \hat{\mathbf{n}}) \, d\partial\mathcal{S} + \int_{\mathcal{S}} \Phi \wedge \mathbf{B} \, d\mathcal{S}, \end{aligned} \quad (97)$$

since  $\sigma$  is symmetric. Using the definition of  $\Phi$ , and following previous developments, this last relation is rewritten

$$\begin{aligned} &\int_{\partial\mathcal{A}_0} \varphi \wedge \int_{h_{\min 0}}^{h_{\max 0}} j \sigma \mathbf{g}^\alpha \, d\xi^3 \nu_\alpha \, d\partial\mathcal{A}_0 + \int_{\partial\mathcal{A}_0} \lambda_h \mathbf{t} \wedge \int_{h_{\min 0}}^{h_{\max 0}} j \xi^3 \sigma \mathbf{g}^\alpha \, d\xi^3 \nu_\alpha \, d\partial\mathcal{A}_0 + \\ &\int_{\mathcal{A}_0} \varphi \wedge [j \sigma \mathbf{g}^3]_{h_{\min 0}}^{h_{\max 0}} \, d\mathcal{A}_0 + \int_{\mathcal{A}_0} \lambda_h \mathbf{t} \wedge [j \xi^3 \sigma \mathbf{g}^3]_{h_{\min 0}}^{h_{\max 0}} \, d\mathcal{A}_0 + \\ &\int_{\mathcal{A}_0 \times [h_{\min 0}; h_{\max 0}]} \frac{\rho_0}{\rho} \varphi \wedge \mathbf{B} \, d\mathcal{A}_0 \, d\xi + \int_{\mathcal{A}_0 \times [h_{\min 0}; h_{\max 0}]} \frac{\rho_0}{\rho} \xi^3 \lambda_h \mathbf{t} \wedge \mathbf{B} \, d\mathcal{A}_0 \, d\xi = 0. \end{aligned} \quad (98)$$

Using definitions (9, 10, 14 and 15) allows simplifying this result into

$$\begin{aligned} &\int_{\partial\mathcal{A}_0} \varphi \wedge \bar{j} \mathbf{n}^\alpha \nu_\alpha \, d\partial\mathcal{A}_0 + \int_{\partial\mathcal{A}_0} \lambda_h \mathbf{t} \wedge \bar{j} \tilde{\mathbf{m}}^\alpha \nu_\alpha \, d\partial\mathcal{A}_0 + \\ &\int_{\mathcal{A}_0} \varphi \wedge \bar{j} \mathbf{n}^{\mathcal{A}_0} \, d\mathcal{A}_0 + \int_{\mathcal{A}_0} \lambda_h \mathbf{t} \wedge \bar{j} \tilde{\mathbf{m}}^{\mathcal{A}_0} \, d\mathcal{A}_0 = 0, \end{aligned} \quad (99)$$

<sup>†</sup>Rigorously, the same results hold for any arbitrary part  $\tilde{\mathcal{A}}_0$  of the Cosserat surface  $\mathcal{A}_0$ .

which becomes after integrating by parts and applying Gauss theorem:

$$0 = \int_{\mathcal{A}_0} \varphi_{,\alpha} \wedge \bar{j} \mathbf{n}^\alpha d\mathcal{A}_0 + \int_{\mathcal{A}_0} \varphi \wedge (\bar{j} \mathbf{n}^\alpha)_{,\alpha} d\mathcal{A}_0 + \int_{\mathcal{A}_0} (\lambda_h \mathbf{t})_{,\alpha} \wedge \bar{j} \tilde{\mathbf{m}}^\alpha d\mathcal{A}_0 + \int_{\mathcal{A}_0} \lambda_h \mathbf{t} \wedge (\bar{j} \tilde{\mathbf{m}}^\alpha)_{,\alpha} d\mathcal{A}_0 + \int_{\mathcal{A}_0} \varphi \wedge \bar{j} \mathbf{n}^{\mathcal{A}_0} d\mathcal{A}_0 + \int_{\mathcal{A}_0} \lambda_h \mathbf{t} \wedge \bar{j} \tilde{\mathbf{m}}^{\mathcal{A}_0} d\mathcal{A}_0. \quad (100)$$

Finally, using (94) and considering the arbitrary nature of  $\mathcal{A}_0$  yields

$$\varphi_{,\alpha} \wedge \bar{j} \mathbf{n}^\alpha + (\lambda_h \mathbf{t})_{,\alpha} \wedge \bar{j} \tilde{\mathbf{m}}^\alpha + \lambda_h \mathbf{t} \wedge (\bar{j} \tilde{\mathbf{m}}^\alpha)_{,\alpha} + \lambda_h \mathbf{t} \wedge \bar{j} \tilde{\mathbf{m}}^{\mathcal{A}_0} = 0 \quad \text{on } \mathcal{A}_0 \quad (101)$$

In order to exploit the symmetric nature of  $\boldsymbol{\sigma}$ , this tensor can be rewritten in the basis  $\mathbf{g}_i$ , leading to

$$\boldsymbol{\sigma} = \sigma^{ij} \mathbf{g}_i \otimes \mathbf{g}_j, \quad (102)$$

which allows to rewrite  $\boldsymbol{\sigma} = \boldsymbol{\sigma}^T$  as  $\mathbf{g}_i \wedge (\boldsymbol{\sigma} \mathbf{g}^i) = 0$ . Using (3) and definitions (9-11), the integration of this relation on the thickness yields

$$\begin{aligned} 0 &= \int_{h_{\min 0}}^{h_{\max 0}} j \left[ \varphi_{,\alpha} + \xi^3 (\lambda_h \mathbf{t})_{,\alpha} \right] \wedge (\boldsymbol{\sigma} \mathbf{g}^\alpha) d\xi^3 + \int_{h_{\min 0}}^{h_{\max 0}} j \lambda_h \mathbf{t} \wedge (\boldsymbol{\sigma} \mathbf{g}^3) d\xi^3 \\ &= \varphi_{,\alpha} \wedge \bar{j} \mathbf{n}^\alpha + (\lambda_h \mathbf{t})_{,\alpha} \wedge \bar{j} \tilde{\mathbf{m}}^\alpha + \lambda_h \mathbf{t} \wedge \bar{j} \mathbf{l}, \end{aligned} \quad (103)$$

which allows to rewrite (101) as

$$\lambda_h \mathbf{t} \wedge (\bar{j} \tilde{\mathbf{m}}^\alpha)_{,\alpha} + \lambda_h \mathbf{t} \wedge \bar{j} \tilde{\mathbf{m}}^{\mathcal{A}_0} - \lambda_h \mathbf{t} \wedge \bar{j} \mathbf{l} = 0 \quad \text{on } \mathcal{A}_0, \quad (104)$$

or again, if  $\lambda$  is an undefined pressure as

$$(\bar{j} \tilde{\mathbf{m}}^\alpha)_{,\alpha} + \bar{j} \tilde{\mathbf{m}}^{\mathcal{A}_0} - \bar{j} \mathbf{l} + \bar{j} \lambda \mathbf{t} = 0 \quad \text{on } \mathcal{A}_0. \quad (105)$$

## List of Figures

1	Description of the different configurations of the shell. . . . .	40
2	Study of the pinched open hemisphere: a) Geometry of the open hemisphere (only one fourth is considered). b) Final deformation of the completed hemisphere for a regular mesh of 8 bi-cubic quadrangular elements on each side. c) Final deformation of the completed hemisphere for a distorted mesh of 8 bi-cubic quadrangular elements on each side. . . . .	41
3	Study of the pinched open hemisphere: force-displacement evolutions of the nodes located at the loadings. Stabilization parameter $\beta = 10^2$ . . . . .	42
4	Study of the pinched open hemisphere: a) Influence of the stabilization parameter on the results at $P=400$ N, for 8 bi-cubic and 12 bi-quadratic elements on each edge. b) Influence of the mesh size on the results at $P=400$ N, for bi-cubic and bi-quadratic elements on each edge, and for $\beta=10^2$ . . . . .	43
5	Study of the pinched open hemisphere: convergence rate with respect to the mesh size on the results at $P=400$ N, for bi-cubic and bi-quadratic elements on each edge, and for $\beta=10^2$ . . . . .	44
6	Study of the thin plate ring: a) Geometry of the initially cut ring (one side of line AB is clamped and the other one is uniformly loaded). b) Final deformation of the test for a regular mesh of 16 bi-quadratic quadrangular elements on the circumference and 3 bi-quadratic quadrangular elements on the edge AB. . . .	45
7	Study of the plate ring: force-displacement evolutions of the nodes located at the cutting. Stabilization parameter $\beta = 10^2$ . . . . .	46
8	Study of the clamped cylinder: a) Geometry of the cylinder (only one fourth is considered). b-f) Final deformation of the test for a regular mesh of 12 bi-quadratic quadrangular elements on each edge, and for $P = 400, 752, 800, 1200$ and 1600 N. Stabilization parameter $\beta = 10^2$ . . . . .	47
9	Study of the clamped cylinder: force-displacement evolutions of the nodes located at point A. Stabilization parameter $\beta = 10^2$ . . . . .	48

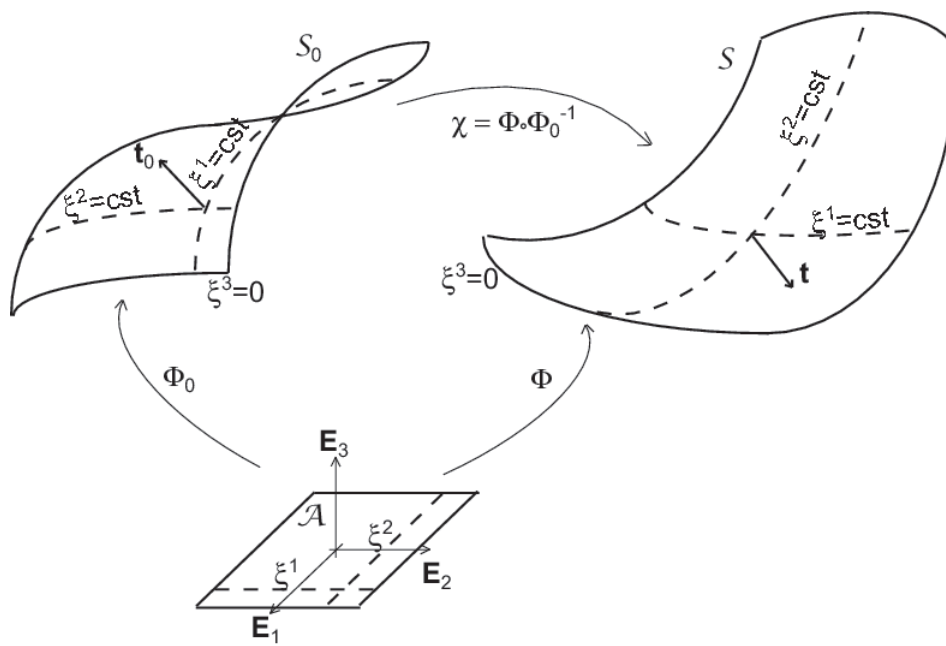


Figure 1. Description of the different configurations of the shell.

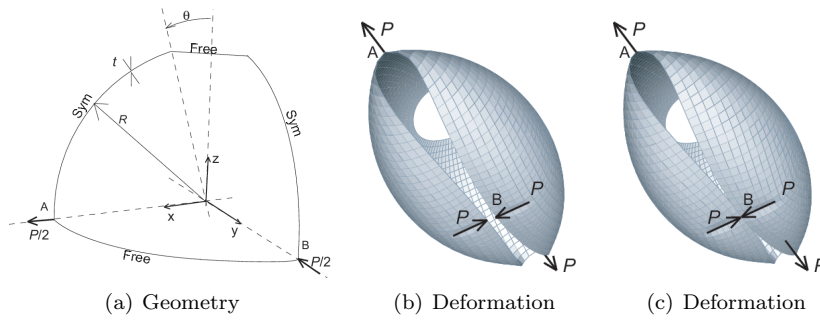


Figure 2. Study of the pinched open hemisphere: a) Geometry of the open hemisphere (only one fourth is considered). b) Final deformation of the completed hemisphere for a regular mesh of 8 bi-cubic quadrangular elements on each side. c) Final deformation of the completed hemisphere for a distorted mesh of 8 bi-cubic quadrangular elements on each side.

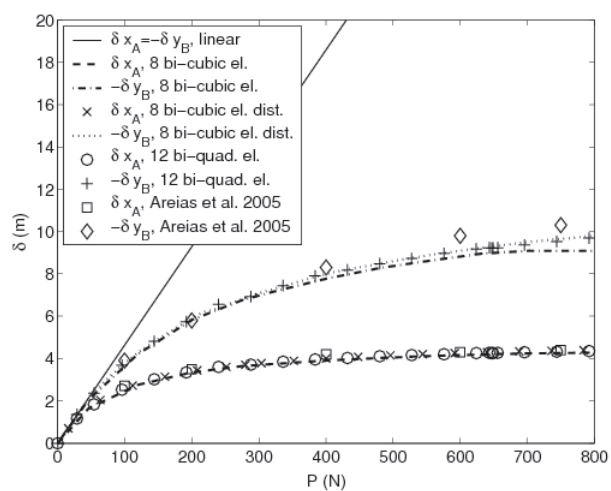


Figure 3. Study of the pinched open hemisphere: force-displacement evolutions of the nodes located at the loadings. Stabilization parameter  $\beta = 10^2$ .

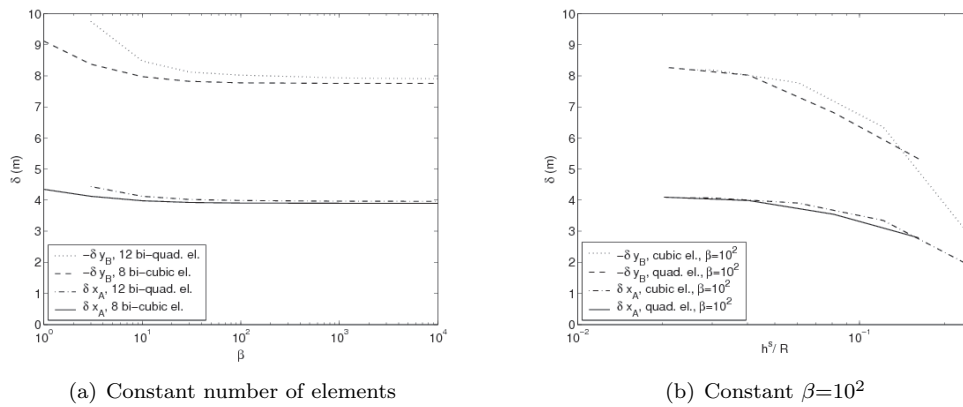


Figure 4. Study of the pinched open hemisphere: a) Influence of the stabilization parameter on the results at  $P=400$  N, for 8 bi-cubic and 12 bi-quadratic elements on each edge. b) Influence of the mesh size on the results at  $P=400$  N, for bi-cubic and bi-quadratic elements on each edge, and for  $\beta=10^2$ .

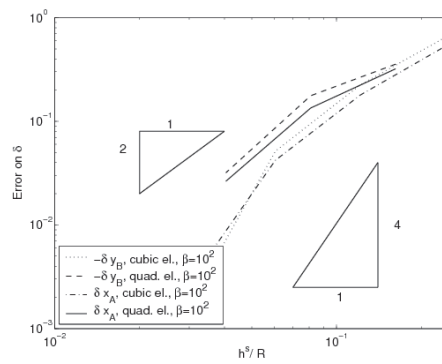


Figure 5. Study of the pinched open hemisphere: convergence rate with respect to the mesh size on the results at  $P=400$  N, for bi-cubic and bi-quadratic elements on each edge, and for  $\beta=10^2$ .

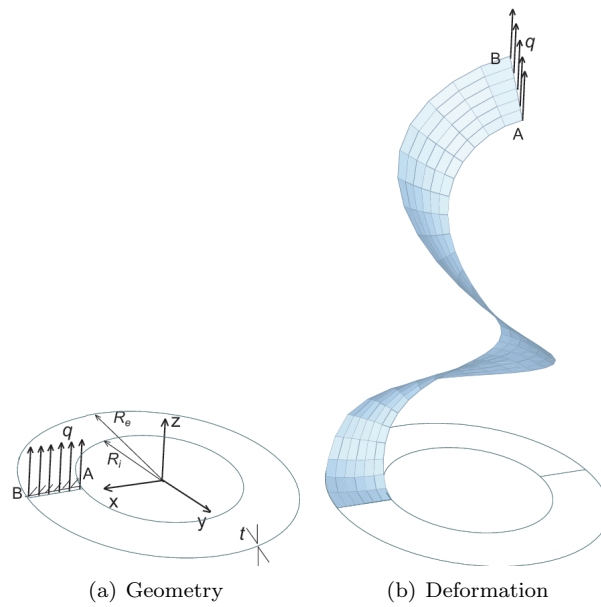


Figure 6. Study of the thin plate ring: a) Geometry of the initially cut ring (one side of line  $AB$  is clamped and the other one is uniformly loaded). b) Final deformation of the test for a regular mesh of 16 bi-quadratic quadrangular elements on the circumference and 3 bi-quadratic quadrangular elements on the edge  $AB$ .

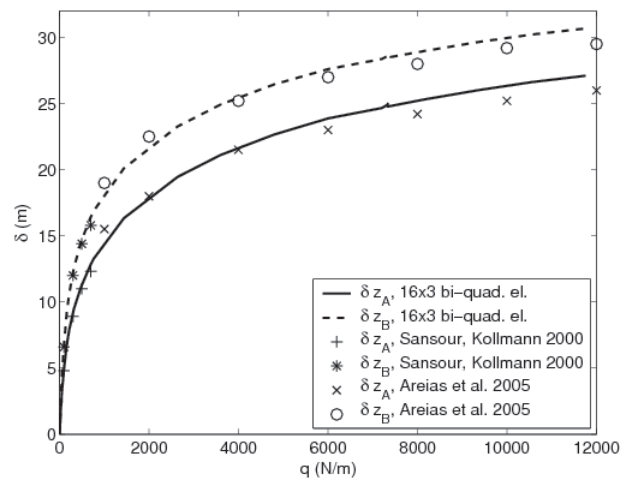


Figure 7. Study of the plate ring: force-displacement evolutions of the nodes located at the cutting. Stabilization parameter  $\beta = 10^2$ .

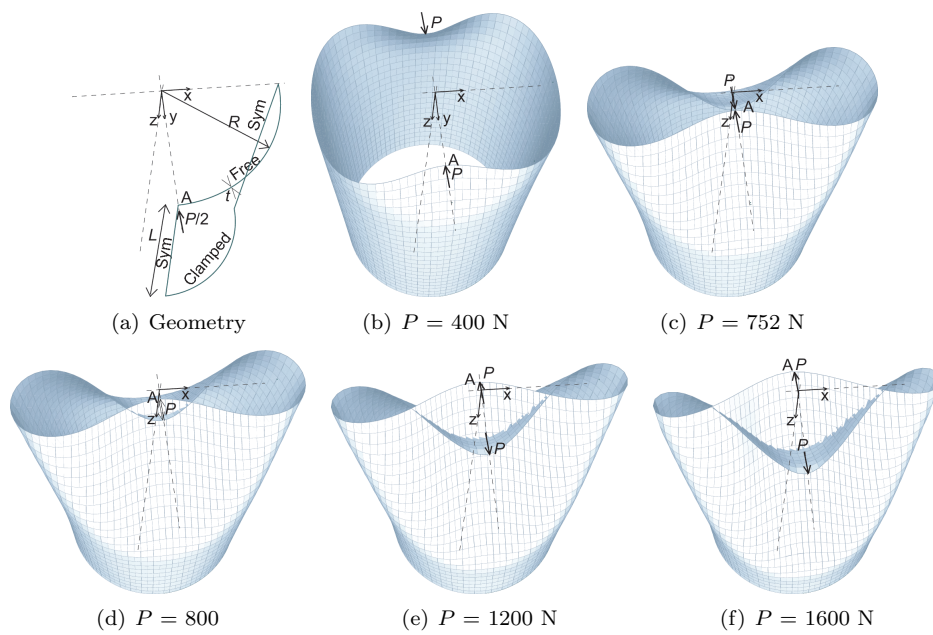


Figure 8. Study of the clamped cylinder: a) Geometry of the cylinder (only one fourth is considered). b-f) Final deformation of the test for a regular mesh of 12 bi-quadratic quadrangul elements on each edge, and for  $P = 400, 752, 800, 1200$  and  $1600$  N. Stabilization parameter  $\beta = 10^2$ .

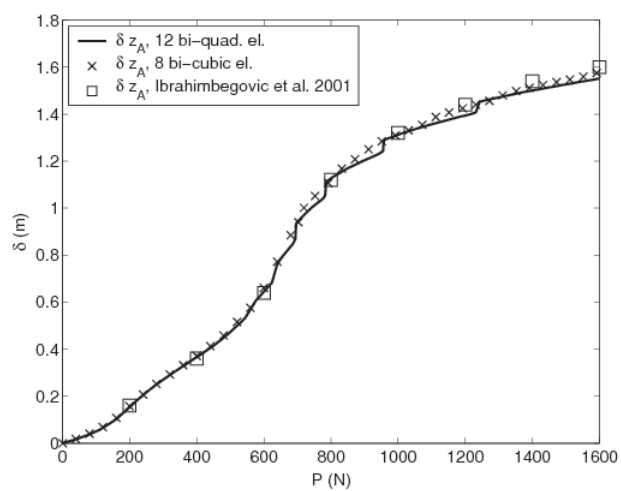


Figure 9. Study of the clamped cylinder: force-displacement evolutions of the nodes located at point A. Stabilization parameter  $\beta = 10^2$ .

## List of Tables

I	Material and geometrical properties for the pinched open hemisphere test. . . .	50
II	Material and geometrical properties for the thin plate ring test. . . . .	51
III	Material and geometrical properties for the clamped cylinder test. . . . .	52

Table I. Material and geometrical properties for the pinched open hemisphere test.

Property	Value
Radius	$R = 10$ m
Thickness	$t = 0.04$ m
Opening	$\theta = 18^\circ$
Young modulus	$E = 6.825 \times 10^7$ N·m <sup>-2</sup>
Poisson's ratio	$\nu = 0.3$
Applied force	$P = 800$ N

Table II. Material and geometrical properties for the thin plate ring test.

Property	Value
Internal Radius	$R_i = 6$ m
External Radius	$R_e = 10$ m
Thickness	$t = 0.03$ m
Young modulus	$E = 2.1 \times 10^{10}$ N·m <sup>-2</sup>
Poisson's ratio	$\nu = 0$
Applied force	$q = 12000$ N·m <sup>-1</sup>

Table III. Material and geometrical properties for the clamped cylinder test.

Property	Value
Radius	$R = 1.016$ m
Length	$L = 3.048$ m
Thickness	$t = 0.03$ m
Young modulus	$E = 2.0685 \times 10^7$ N·m <sup>-2</sup>
Poisson's ratio	$\nu = 0.3$
Applied force	$P = 1600$ N